PERFORMANCE OPTIMIZATION OF TIN HALIDE PEROVSKITE SOLAR CELLS VIA NUMERICAL SIMULATION

A Thesis presented to the Department of

Theoretical Physics

African University of Science and Technology, Abuja

In Partial Fulfilment of the Requirements

For the Degree of

MASTER OF SCIENCE

By

Amu, Tochukwu Loreta

Abuja, Nigeria

December, 2014

PERFORMANCE OPTIMIZATION OF TIN HALIDE PEROVSKITE SOLAR CELLS VIA NUMERICAL SIMULATION

By

Amu, Tochukwu Loreta

A THESIS APPROVED BY THE THEORETICAL PHYSICS DEPARTMENT

RECOMMENDED: ……

Supervisor, Dr. Akin-Ojo Omololu

…….

Head, Department of Theoretical Physics

APPROVED: ……

Chief Academic Officer

……..

Date

ABSTRACT

Organic-inorganic hybrid perovskite solar cells have attracted great attention in the photovoltaic research community in recent years due to its ease of processing, low cost of production, superb light-harvesting characteristics, and relatively high efficiency which make it more preferable over other existing solar cell materials. Lead-based perovskites ($CH_3NH_3PbX_3$, X= Cl, I, Br) solar cells have recently attained a high efficiency of ~19.3% which far surpasses the efficiencies of most thin film and organic solar cells. Therefore, the presence of lead, which is a toxic material in these solar cells poses serious challenge to our health and environment. 'Tin' is non-toxic and stands as a replacement to 'lead' for commercial purposes. Thus, there is a drive to use non-toxic materials such as tin-based perovskites. Unfortunately, the tin-based perovskite solar cells recently produced have low efficiencies ($\leq 6.4\%$). In order to improve the performance of tin-based perovskite solar cells, a numerical simulation was done. First, known experimental results were reproduced. Based on the work reproduced we developed a new configuration with a reduced acceptor doping concentration of the absorber layer which showed an increase in efficiency > 18%. A device simulator, the Solar Cell Capacitance Simulator (SCAPS) was used to solve the poisson and hole and electron continuity equations in order to obtain information concerning the device properties of the tin-based perovskite ($CH_3NH_3SnI_3$) solar cells.

ACKNOWLEDGEMENT

I want to appreciate the following individuals whom God used to make this work a success and my stay in AUST worthwhile. I appreciate my supervisor Dr. Omololu Akin-ojo for his encouragement, contributions, tireless work with me and practically inculcating in me time management principles. I would want to thank Mr. Egidus who followed me up right from the conception of this work to its full realization.

I am also grateful to Prof. Marc Burgelman and his co-workers, Department of Electronics and Information Systems, University of Gent, Belgium for the development of the SCAPS software package and allowing its use. Also, for his useful contributions and prompt response to questions.

My gratitude goes to a mother and a mentor Prof. R.U. Osuji through whom I knew of the existence of AUST and also to African Capacity Building Foundation (ACBF)/BOVAS/NMI for granting me scholarships into this institution, I say I am immensely thankful to all of you.

I would want to appreciate the following group of people for their prayers, admonitions and spiritual supports; members of my Home cell fellowship, my Pastor and his wife (Pst. & Mrs. Nwaka), and my Spiritual Father Bishop David O. Oyedepo.

Special thanks to my entire course mates for taking me like their only sister, encouraging me and also took decisions just to favour me. I want to say I love working with you guys as a team.

Finally, to all my friends, relations and the entire AUST community, I say a big thank you to all of you for being part of my life in AUST.

DEDICATION

I am most grateful to God Almighty without whom I would not have seen the light of the day. Also, for bringing all his promises towards me in this programme to come to fulfilment with sound mind and good health.

To my Father and Mother (of blessed memory) who nurtured me into a full grown adult. Taught me morals and never ceased praying for me at all times. To my siblings, for their encouragements, cautions and financial supports all through my stay here.

Finally, to these great friends of mine, Aina, Toyin, Nwankwo, Udoka and Onah Emenike whom God used to morally support and encourage me into believing in myself and always assuring me that I can do it, even when all hope was lost and almost gave up.

TABLE OF CONTENTS

LIST OF FIGURES

LIST OF TABLES

CHAPTER ONE

INTRODUCTION

1.1 General Background

The limited resources of conventional nonrenewable energy sources such as gas, coal and petroleum, along with the growing opposition to nuclear power generation, motivated by concerns about safety issues and radioactive waste disposal, have led to an increasing demand for safer, cleaner, and, most importantly, renewable sources of energy. Photovoltaic (PV) technologies offer such a solution and have already been used for many years [1]. Initially, the use of PVs was for power generation on satellites and space crafts [2] and later also for terrestrial applications [3] .

The population growth, which is particularly large in off-grid rural areas not connected to the state electrical networks (about 2.5 billion worldwide [4]), is another factor favoring the development of the PV industry. The interest in solar cells as an alternative energy source for terrestrial applications is further driven by social concerns about modern improved living standards as well as the high human desire to save money. There is also a need to protect our health and environment. These can be achieved through the use of energy that is produced from environmentally-benign PV technology, instead of the conventional fossil fuels, which produce environmentally-harmful greenhouse gases[5].

The promising PV potentials above have increased research interests and concerns on the sustainability and use of PV systems in solving global energy deficiencies [6]. These have resulted not only in the further improvement of the efficiencies of silicon solar cells [7] along with considerable reduction of the solar energy cost, but also in the development of new PV materials and novel solar cell devices. The increase in production volume and new cost efficient solar cell technologies rendered this achievement possible. Currently a number of promising options for future developments of PV technology are available. The commercialization of these technologies has been hindered by the high cost per peak watt of solar cell modules. Even though researchers have made efforts over the years, improved performance, lower costs and reliability

of PV systems remain major concerns [8]. Hence, policy goals by state agents pertaining improved energy security and diversity, reduced emissions of greenhouse gases and increased levels of technology growth have spawned PV technologies in the past years.

1.2 The Sun and Solar Radiation

The sun, our closest star, is the origin of most of the energy maintaining life on earth and produces the necessary gravitational attraction to keep our planet in a nearly circular orbit. It has a mass of 1.99 x 10^{30} kg and a radius of 6.96 x 10^{8} m [9]. The earth-sun distance, R, is approximately 1.5 x 10^{11} m. A simple model assumes that the sun is spherical and the spectrum of the Sun's solar radiation is close to that of a blackbody [10],[11] whose surface temperature is at about T ≈ 6000 K. This surface temperature is maintained by energy generated through continuous nuclear fusion of hydrogen into helium in the interior. The interior temperature is, approximately 10^{7}K. As a result of interior temperature, the surface (photosphere) radiates electromagnetic waves in all directions. The spectral distribution is changed considerably when the sunlight penetrates through the earth's atmosphere. Even for a clear sky, the light intensity is attenuated by at least 30% due to scattering by molecules, aerosols and dust particles and adsorption by its constituent gases like water vapor, ozone or carbon dioxide.

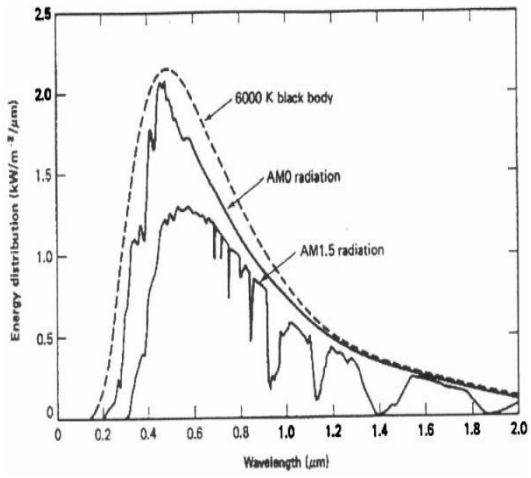

Figure 1.1: Solar irradiance spectrum

The figure above shows the radiations outside the earth's atmosphere (AM0) and at the surface (AM1.5). The dashed line in fig. 1.1 indicates the radiation distribution expected from the sun if it were a perfect blackbody at a temperature of 6000 K [9].

1.2.1 The Air Mass (AM)

The degree of attenuation is highly variable because of the constantly changing position of the sun and the corresponding change of the light path through the atmosphere. These effects are conveniently described by defining an air mass number (AMm). Air mass according to IEEE Standard Dictionary of Electrical and Electronics Terms [12] is the mass of air between a surface and the sun that affects the spectral distribution and intensity of sunlight. Air mass is the relative path length of light through the earth's atmosphere in relation to the zenith point (Fig.1.2); the zenith point is the path length vertically upward at 90^0 and is defined as AM1. Hence, AM1 is the spectral distribution and intensity of sunlight on earth at sea level with the sun directly overhead and passing through a standard atmosphere. AM0 is the spectral distribution and intensity of sunlight outside the earth's atmosphere. Air mass 0 is above the earth's atmosphere along the zenith point. Solar cells are tested at AM1.5, which corresponds to the sun at a 48.2^0 from the zenith point, with a temperature of 25 ^{0}C. For any given angle θ, with respect to the overhead position, the air mass takes the value AMm, in which the air mass number, m, is represented as $m = 1/\cos\theta$ and thus measures the atmospheric path length relative to path length when the sun is directly overhead. AM2 is the solar radiation at ground level when the sun is 60.1° above the horizon. The most widely used terrestrial standard is the AM1.5 spectral distribution (for $\theta = 48.2°$), which is plotted as the terrestrial curve in Fig. 1.1. This terrestrial standard allows a meaningful comparison of different solar cells tested at different locations [13]

.

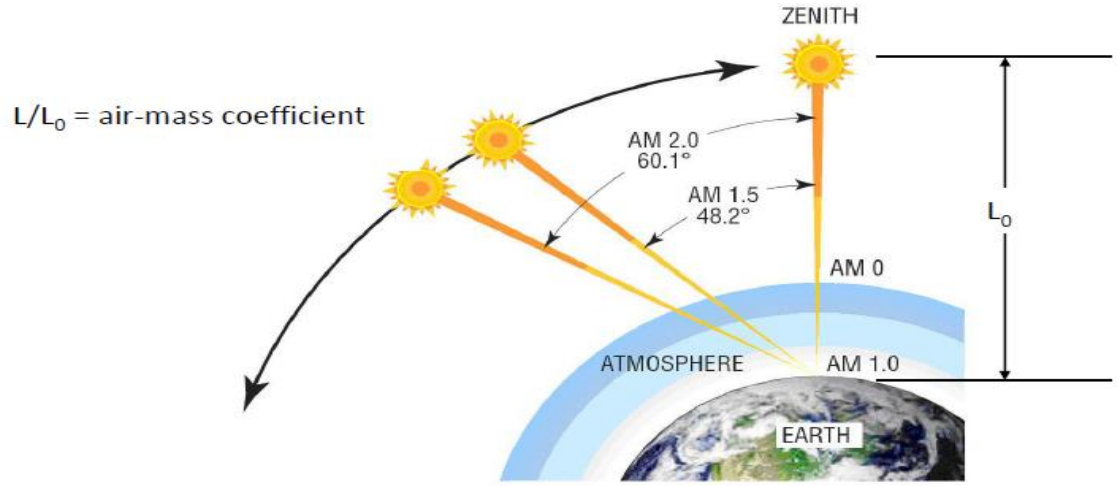

Figure 1.2: Illustration of various air mass (AM) positions and the zenith point. [Adapted from M.Pagliaro et al. (2008)].

1.3 The Solar cell

An example of a solar cell is a p-n junction semiconductor device which converts the solar energy (sunlight) directly into electricity by the photovoltaic effect. Solar cells are described as being photovoltaic irrespective of whether the source is sunlight or an artificial light. The operation of a PV cell is based generally on the following three steps:

1. The absorption of light, generating electron-hole (exciton) pairs.
2. The separation of excitons into free charge carriers (electrons and holes).
3. The transportation of separated charge carriers to their respective anode and cathode of the solar cell, and extraction of those carriers to an external circuit.

1.3.1 Evolution of Solar Cells

The advancement in solar cell technology is in order to produce a cheap (easy to produce), high efficiency and long lifetime (stable) solar cell which is a better replacement for energy generation from fossil fuel. Research has been going on, in order to meet these ultimate goals in photovoltaic technology which has led to the discoveries of new materials and new techniques in solar cells fabrication. Solar cells are categorized into three main groups known as generations based on their order of appearance in the market [14] .

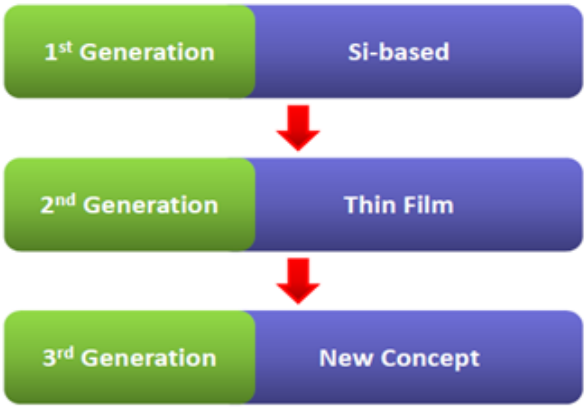

Figure1.3: A schematic representation of the Evolutions of Solar cells Technology

1.3.1.1 First generation

The solar cells in this category are mainly made of silicon wafer. Bell Laboratories developed the first silicon solar cell in 1954 [15], [16] with an efficiency of 6%. Since then, research on improving the efficiency and lowering the cost of these solar cells has been abundant. Silicon solar cells are the most widely used of all solar cells, and they are also the most efficient in terms of single crystalline cell photovoltaic devices. Also, silicon is the most abundant element on earth, only second to oxygen. This type of solar cell is the most widely used with the highest reported cell efficiency (single crystal cell) of ~ 28% [17]. There are three types of silicon, used in this generation of solar cells: single crystalline silicon (c-Si), multicrystalline silicon and amorphous silicon (a-Si). However, c-Si is expensive and involves high cost of fabrication. This has increased recent research interests into the next generation of thin film solar cells.

1.3.1.2 Second generation

This is also known as thin film solar cells. In an effort to reduce the fabrication costs of the present technology based on Si, and to increase material utilization, thin film materials have been the subject of intensive research. This second generation materials had been developed to reduce production costs of solar cells without jeopardizing their energy output [14]. Three main types of materials have emerged as the most promising candidates for this generation of solar cells. These are hydrogenated amorphous silicon (a-Si:H), cadmium telluride (CdTe) as well as copper indium diselenide ($CuInSe_2$) and its related alloys like Copper Indium Gallium diselenide

$CuIn_xGa_{1-x}Se_2$ (CIGS). The highest recorded efficiencies of CIGS and CdTe thin film single cells are as high as 20% and 17%, respectively [13][18].

Although these thin film solar cells have a competitive edge on the first generation solar cells because of lower costs and good efficiencies, they have some drawbacks. Most of the material that these cells are made of are both becoming increasingly rare and more expensive (indium) or are highly toxic (cadmium). To mass produce these solar cells would also require new facilities, which would greatly increase the cost of production. Because of these drawbacks, a different generation of solar cells has been inspired[13].

1.3.1.3 Third generation

This generation of solar cells includes new concepts in their development. These new concepts are in order to solve the major challenges facing the first and second generation of solar cells which are the high costs of first generation solar cells and toxicity and limited availability of materials for second generation solar cells. This new generation includes Organic/polymer and dye-sensitized solar cells. Organic photovoltaic solar cell (OPV) technology employs semiconducting polymers as low cost materials alternatives to inorganic photoactive semiconductors (silicon, CdTe and CIGS). The third generation of solar cells is the cheapest of all the other solar cell generations. The efficiencies gotten so far for dye-sensitized and polymer single cells are ~ 11% and 8% respectively. This indicates that the efficiency of organic solar cell generation is generally very low. Furthermore, organic photovoltaic is technologically immature and its wide spread applications are limited by several instabilities issues that are associated to its solar cell degradation mechanisms in different environments. Hence, OPV and dye-sensitized technology are relatively low to make these cells competitive in a commercial market [13].

With the relentless effort of researchers in photovoltaics, a new type of solar cell which is based on organic-inorganic hybrid solar cell known as perovskite was discovered in 2006 by Miyasaka and his co-workers [19], [20]. This new material has a highest reported efficiency of ~19.3% [21]. These hybrid solar cell technologies such as perovskite based solar cells are classified as such because their photoactive layer is made of organometallic material. This work will focus purely on this organic-inorganic perovskite based solar cell which also shall be limited to a particular type known as methylammonium tin tri-iodide ($CH_3NH_3SnI_3$).

1.4 Motivation

At present, the perovskite based solar cells are regarded as promising candidates of hybrid solar cells due to their ease of fabrication, strong solar absorption coefficient and low non-radiative carrier recombination rates for such simply prepared materials, plus its ability to capitalize on over 20 years of development of related dye-sensitized and organic photovoltaic cells [22]. Recent results in literature suggest that a vapour-deposition [23] and a sequential solution deposition route [24] approaches are required to yield good quality films and high efficiency ($\eta \geq 15\%$) solar cell devices for lead perovskite. However, the presence of lead in the most efficient ones which contain $CH_3NH_3PbI_3$ poses a serious challenge to the continued adoption of lead perovskite solar cells for commercial purposes due to the toxicity of lead which is a key component in this perovskite. This has led to a search for a non- toxic substitute for lead. Tin can be a viable substitute for lead since it is non-toxic and also in the same group as lead in the periodic table. Also, the relatively high absorbance of lead-free perovskite solar cells has demonstrated that its performance is not linked to the presence of lead and also beckons even higher efficiencies for non-toxic, abundant low cost solar cells [25]. The highest efficiencies of tin- halide perovskite as reported by [25] is 6.4%.

1.5 Objectives of the research

Though Sn based perovskite solar cells are non-toxic compared to their lead counterparts, they cannot be directly used to replace lead perovskite solar cells. This is due mainly to their low efficiency, which makes them not as competitive as lead containing perovskite solar cell systems. Therefore, tin-based perovskite solar cells require efficiency improvements prior to their acceptability for applications in terrestrial energy production. Hence, the contribution of this study is to explore ways in which the efficiency of Sn-based perovskite can be improved. A numerical simulation approach will be used to study the characteristics of tin-based perovskite solar cells that are relevant for their performance improvement.

Our study is guided by the following specific objectives:

- Develop a planar architecture of a tin-based perovskite solar
- Reproduce the experimental result using our developed architecture
- To investigate the influence of interlayer properties on the performance of the solar cells.

- Improve the efficiency of the obtained result

1.6 Research Methodology

The method adopted in this work is totally computational modeling. The results obtained will be compared with the experimental data that were reported earlier by Noel *et al*.[25]. Attempts will be made to optimize the layer thicknesses in order to improve the performance of the solar cell. The modeling is carried out using a numerical software package called Solar Cell Capacitance Simulator (SCAPS). SCAPS [26] is a 1D numerical simulation program developed at University of Gent, Belgium. This is used to predict the changes in Sn-perovskite based solar cell performances associated to the incorporation of the absorber and the buffer (TiO_2) layers. An optimum value of the absorber thickness will be determined.

Due to the short diffusion length (L_n) of ~30nm of the charge carriers of the absorber as reported by [25], there is bound to be recombination of charge carriers generated in the absorber, if the absorber thickness is larger than $L_{n.}$ In that case, the charges recombine before they get extracted at the electrodes [27]. This causes loss of charges and hence low solar cell efficiency. Reducing the thickness of the absorber can minimize this recombination effect. Furthermore, the different device parameters will be computed. These include the efficiency η, fill factor FF, short circuit current J_{sc} and the open circuit voltage V_{oc}. These will also be compared with the experimental results in the literature[25], [28]

1.7 Scope and Organization of the Study

This thesis is organized into five chapters. In Chapter 2, a literature survey is presented on the relevant theoretical aspects of present research. The typical solar cell designs are presented along with the advantages of perovskite solar cells. Attention is also focused on the critical relationship between the material properties and the fabrication conditions of these solar cells.

In Chapter 3, the numerical modelling of the device structure is performed based on a planar heterojunction device architecture. The results obtained are compared with experiments from literature [25]. In chapter 4, a detailed result analysis is carried out and presented. Finally, in Chapter 5, the most significant results are summarized. Concluding remarks and suggestions for future work are also presented in this chapter of the report.

CHAPTER TWO

LITERATURE REVIEW

2.1 Working principle of photovoltaic solar cells

The working principle of all solar cells is essentially based on the 'photovoltaic effect'. In general, the photovoltaic effect means the generation of a potential difference at the junction of two different materials in response to visible or other radiation. Therefore, a cell is a two terminal device which conducts like a diode in the dark and generates a photovoltage when illuminated by the sun[29].

A simple photovoltaic cell is the p-n junction shown in fig. 2.1a below. A p-n junction device in the dark, exhibits the characteristics of a rectifier diode. The J-V characteristic curves in Fig.2.1b shows a p-n junction in dark and under illumination.

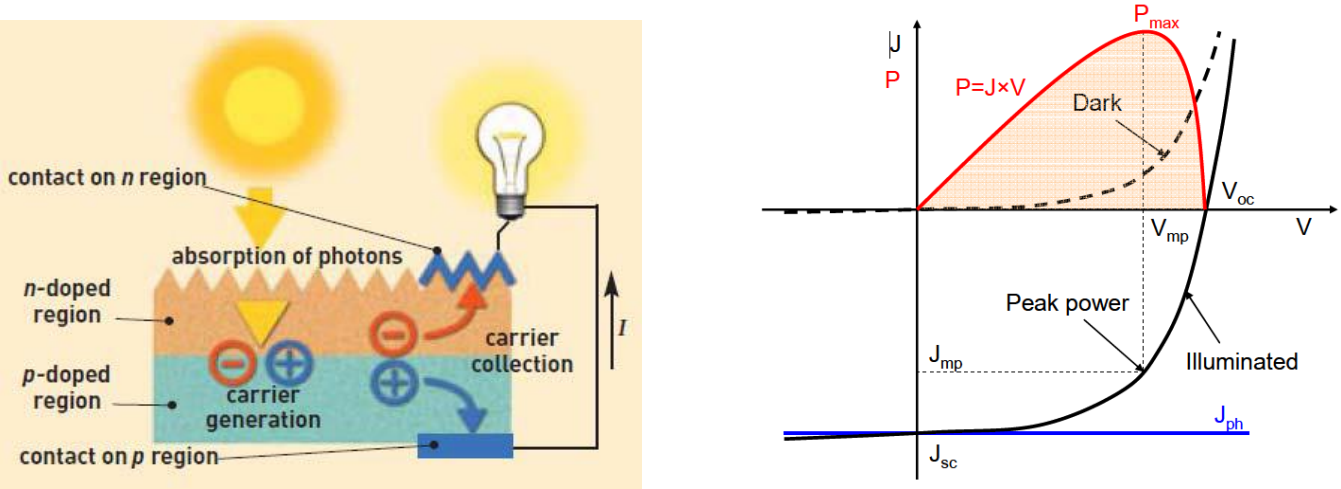

(a) (b)

Figure 2.1: (a) A typical p-n junction solar cell (b) J-V characteristics of a p-n junction in the dark and under illumination. Adapted from Ref.[27]

2.2 Solar cell device characterization parameters

The main parameters that are used to characterize the performance of solar cells are the peak power, P_{max}, the short-circuit current density, J_{sc}, the open-circuit voltage, V_{oc}, and the Fill Factor, FF. These parameters are determined from the illuminated $J-V$ characteristic curve as illustrated in Figure 2.1b. The conversion efficiency, η, is determined from these parameters.

Brief explanations and formulae for these parameters are given below for a simple p-n junction device.

2.2.1 Short-Circuit Current Density, J_{sc}

The short-circuit current density is the maximum photo-generated current delivered by a solar cell when the terminals of the solar cell are in contact with each other (i.e. short-circuited). The solution for J_{sc} can be gotten from the net current density $J(V)$ in the solar cell given as [27]

$$J(V) = J_{sc} - J_{dark}(V), \tag{2.1}$$

where

$J_{dark}(V)$ is the dark current density. This is given by:

$$J_{dark}(V) = J_o\left(e^{qV/mK_BT} - 1\right) \tag{2.2}$$

Under illumination, the solar cell behavior is described using the ideal diode equation (2.2) and an additional current source J_{sc} due to illumination. Thus, with the electronic charge $(q = 1.603 \times 10^{-19}C)$ and Boltzmann's constant $(K_B = 1.38 \times 10^{-23}JK^{-1})$, the illuminated solar cell equation is given by

$$J(V) = J_{sc} - J_o\left(e^{qV/mK_BT} - 1\right) \tag{2.3a}$$

Or equivalently, the short circuit current given by:

$$J_{SC} = J(V) + J_0\left(e^{qV/mK_BT} - 1\right) \tag{2.3b}$$

Where V is the voltage across the junction, T is the absolute temperature, J_0 is the dark saturation current density and m is the ideality factor with values between 1 and 2,[27].

2.2.2 The open-circuit voltage, V_{oc}

V_{oc} is the voltage at which no current flows through the external circuit when the terminals of the solar cell are not connected to each other. It is the maximum voltage that a solar cell can deliver. The V_{oc} depends on the photogenerated current density, J_{ph}. For the simple p-n junction, It is given by [27]:

$$V_{oc} = \frac{mK_BT}{q} In\left(\frac{J_{ph}}{J_o} + 1\right) \quad (2.4)$$

This is obtained from equation (2.3b) by setting the net current, J(V) to zero. This leads to compensation effect between the dark and the photocurrent, such that $J(V) = 0, J_{sc} = J_{ph}$ and $V = V_{oc}$.

2.2.3 Fill factor, FF

The fill factor is the ratio between the maximum power $(P_{max} = J_{mp} \times V_{mp})$ generated by a solar cell and the product of V_{oc} and J_{sc}. FF describes the 'squareness' of the J-V curve.

$$FF = \frac{V_{mp} J_{mp}}{V_{oc} J_{sc}} = \frac{P_{max}}{V_{oc} J_{sc}} \quad (2.5)$$

V_{mp} and J_{mp} are the maximum point voltage and current density generated by a solar cell (Figure 2.1b).

2.2.4 Power Conversion Efficiency, η

The power conversion efficiency is calculated as the ratio between the generated maximum power and the incident power. This is given by:

$$\eta = \frac{P_{max}}{P_{in}} = \frac{J_{sc} V_{oc} FF}{P_{in}} \quad (2.6)$$

The irradiance value, P_{in} of 1000 W/m^2 of AM1.5 spectrum has become a standard for measuring the conversion efficiency of solar cells. Where the irradiance power,P_{in}, is the standard incident power as function of solar cell area. It has a value of $1000\ W/m^2$ of $AM1.5$ spectrum[27].

2.3 Junctions in solar cell device

Junctions in solar cell devices are the interfaces between the semiconductor materials that make up the solar cells or semiconductor and other materials. For example, the regions that form between the p-type and n- type semiconductor materials result in internal electric fields being generated. These fields are especially important in the separation of charge carriers which drift in opposite directions to the metal contacts (electrodes). As mentioned already, these junctions are

known as p-n junctions [27]. Other junctions that are relevant in solar cell designs, include the p-i-n and the metal-semiconductor junctions[29].

2.4 Perovskite solar cells

In an effort to develop cost-effective photovoltaic systems alternatives to silicon solar cells, perovskite-based solar cells have attracted considerable interest Ref.[22]. These have increased the efficiencies of perovskite solar cells to high levels, surpassing the efficiencies of many commercial photovoltaics, such as dye-sensitised Ref.[30], organic Ref.[30] and amorphous silicon solar cells [31]. Furthermore, the efficiency of perovskite based solar cells compares favorably with most of photovoltaic systems that are used currently in the solar cell industry (Figure 2.2).

A perovskite material refers generally to any material with crystal structure of the form ABX_3 (Figure 2.3), same as calcium titanium oxide, $CaTiO_3$. Here X is an anion, A and B are cations of organic or inorganic material of different sizes (A being larger in size than B)[22].

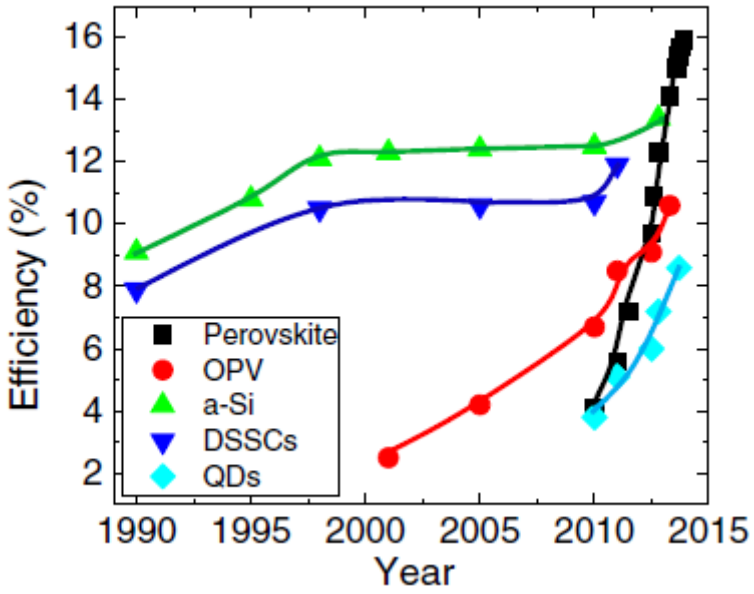

Figure 2.2: Efficiency evolution of different solar cells photovoltaic technologies. Adapted from Ref. [26]

The structure of the perovskites currently used in solar cells consists of a network of corner-sharing BX_6 octahedra with the B cation (typically Sn^{2+} or Pb^{2+}) and X is a halogen typically F^-, Cl^-, Br^- or I^-. The cation A is selected to balance the total charge and it can be an

organic (eg. Methylammonium $CH_3NH_3^+$, Formamidinium $NH_2CH{=}NH_2^+$) or inorganic material like Cs^+ ion [32], [33]. Perovskites are well known for their phase complexity, with accessible cubic, tetragonal, orthorhombic, trigonal and monoclinic polymorphs depending on the tilting and rotation of the BX_6 polyhedra in the lattice [34]. Phase transitions are frequently observed in lead perovskites under the influence of temperature, pressure and/or applied electric field[35].

$MASnI_3$ perovskite possesses a tetragonal crystal structure just like the $MAPbI_3$ but under different temperature[36] with the lattice parameters a = 8.7912 Å and c = 4.4770 Å. $MASnI_3$ holds the following optical and electrical properties which makes it viable for photovoltaic applications. A small optical band gap of 1.23eV, broad absorption edge of ~1000nm and an excellent hole transporter [37].

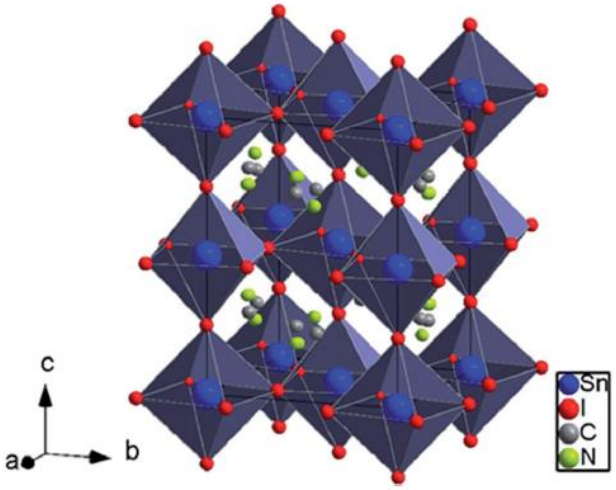

Figure 2.3: Tetragonal structure of MASnI3. Adapted from Ref. [32]

2.4.1 Properties of organic-inorganic hybrid perovskite materials

Perovskite materials are widely used as photoabsorbers in perovskite based solar cells. The interest in organic-inorganic hybrid perovskite materials has been due largely to their interesting characteristics of the inorganic components, which include thermal stability[38] and the high degree of structural order[38] and also due to the properties of the organic component such as the functional versatility, mechanical flexibility and low-cost processability [39][40]. Hence, the possibility of merging the properties of typical inorganic crystals with those of molecular organic solids has stimulated recent research into the versatile properties of organic-inorganic hybrid perovskite materials.

In more details, organic-inorganic hybrid perovskite materials have some enticing potential for applications in photovoltaic devices. Which include:

1) Excellent light-harvesting characteristics[20], [23] as well as good hole transporting properties [41].
2) Potentially low processing cost.
3) Low temperature solar cell processing preferably via the printing techniques[38], which makes it possible to be deposited on a flexible substrate [38],[42].
4) It increases light absorption, thus increasing the photogeneration of free charge carriers. This enables low energy-loss by the charges generated and increase their collection at the electrodes.[43], [44].
5) Low energy payback time due to low processing cost and high efficiency. Energy payback time is the time or duration it takes for solar cells to give back the equivalent energy used or expended on its production. A low payback time can be achieved in a material with low cost of production and high performance.

Despite these advantages of organic-inorganic hybrid perovskites, there are generally four major challenges facing perovskite solar cells, which hinder their commercialization. Researchers have worked on addressing some of these challenges in various capacities. These efforts have proffered solutions in overcoming them. These problems include:

- Perovskite materials are extremely sensitive to oxygen and water vapor, which degrade the solar cells by dissolving the salt-like perovskite crystal structure. This has been addressed by preparing the perovskite thin films in an inert atmosphere such as Nitrogen [25],[28] or Argon [35] filled glove boxes. This is followed with immediate encapsulation of the whole device within an air tight sealant with the same inert condition. Although it is not cost effective for large scale production, this method has been used to reduce the degradation of tin perovskite and oxidation of Sn^{2+} to Sn^{4+}. Thus increasing the solar cell lifetime for a period of 4-months for tin perovskite [25].
- It is challenging to prepare large continuous films in glove boxes, which limits it for large scale production of perovskite solar cells. However, sequential deposition of the constituents components perovskite materials can be used to get a continuous film over a larger area without degradation of the cell efficiency [24].

- Lead, which is the most-used perovskite solar cells, is toxic. This could leach out of the solar panel into the environment causing health and ecological challenge. Hence, environmentally-benign element such as tin has recently been proposed as solar cell materials alternatives to lead perovskites.
- Low lifetime due to phase transition: the longer-term stability of perovskite solar cells has not been verified. There are a few studies on storage lifetime. However, they are only limited on an operating cell (under illumination at the maximum power) sealed at ~45°C ambient temperature [24]. In that, study, the authors observed a decrease in initial solar cell power conversion efficiency of less than 20% after 500 h.

While much work has been done on lead halide perovskite solar cells, there are relatively few reports on tin halide perovskite solar cells. Much experimental efforts have been made in addressing the problems listed above; the optimization of tin halide perovskite solar cells with accent on their efficiencies has not been fully examined. There is also a need to develop models and numerical simulations complements to experiments, which are relatively difficult to understand. Therefore, this work will use numerical modeling to obtain insight into the details of the physical operation of thin-film organic-inorganic hybrid tin perovskite solar cells with planar-interface heterojunction structure.

2.5 Prior work on the organic-inorganic hybrid perovskite solar cells

Single and mixed halides perovskite such as $CH_3NH_3PbI_3$ and $CH_3NH_3PbI_{3-x}Cl_x$ have recently been used as light harvesters[22]. Due to their high light absorption coefficients, these materials have been shown to have resulted in solar cells with efficiencies of over 15% [23], [45]. Furthermore, an efficiency of 17.9% has been recently recorded by Soek et al. [46] who produced a perovskite solar cell with mixed-halide $CH_3NH_3PbI_{3-x}Br_x$ using poly-triarylamine as hole transport material (HTM).

However, lead being a toxic element has really been a concern [47]. In an effort to address this concern, tin has been proposed for effective replacement of lead. Kanatzidis et al.[28] have reported on lead-free perovskite solar cell that was based on methylammonium tin iodide ($CH_3NH_3SnI_3$). They observed a decrease in Voc as compared to lead-containing perovskite solar cell devices with the same configuration. Also, these authors [28] have investigated the possibility of using a mixed halide of $CH_3NH_3SnI_{3-x}Br_x$ as the light- absorbing

material in solution-processed solid-state photovoltaic devices. The mixed halide was tried in realization of its tunable band gap, which should allow increases in V_{oc} of the devices. For comparison, Table1 summarizes some important results obtained in Ref.[28]. In a different work, with a similar $CH_3NH_3SnI_3$ perovskite material having a slightly lower bandgap energy of 1.23 eV, Snaith *et al.*[25] reported a solar cell with efficiency of 6.4%.

Table 2.1: Optical band gaps and refined lattice parameters of the ABX_3 (x = 0, 1, 2, 3) perovskites and their corresponding solar cell performance parameters[28]

Perovskite	Bandgap (eV)	J_{sc} (mA cm^{-2})	V_{oc} (V)	FF	η (%)
CH_3NH_3 SnI_3	1.30	16.30±0.71	0.68±0.03	0.48±0.03	5.23±0.18
CH_3 NH_3 SnI_2 Br	1.56	14.38±0.49	0.77±0.02	0.50±0.02	5.48±0.15
CH_3 NH_3 $SnIBr_2$	1.75	12.30±0.47	0.82±0.03	0.57±0.02	5.73±0.23
CH_3 NH_3 $SnBr_3$	2.15	8.26±0.53	0.88±0.03	0.59±0.02	4.27±0.18

2.5.1 Perovskite solar cells device architecture

Perovskite solar cells have been produced using different device structures, shown in Figure 2.4. These show the possible ways that have been recently used in the design and fabrication of perovskite solar cell devices with different performance. For numerical modeling and simulation, it is straightforward to use the solar cell configuration in fig.2.4(c). The later has the structure of a thin-film p-i-n solar cell with planar heterojunction structure. This allows the use of numerical software packages such as Solar Cells Capacitance Simulation (SCAPS)[48] for modeling and numerical characterization of perovskite solar cell devices, in a way similar to the structure of thin-film compound semiconductor solar cells, such as CIGS [49] .

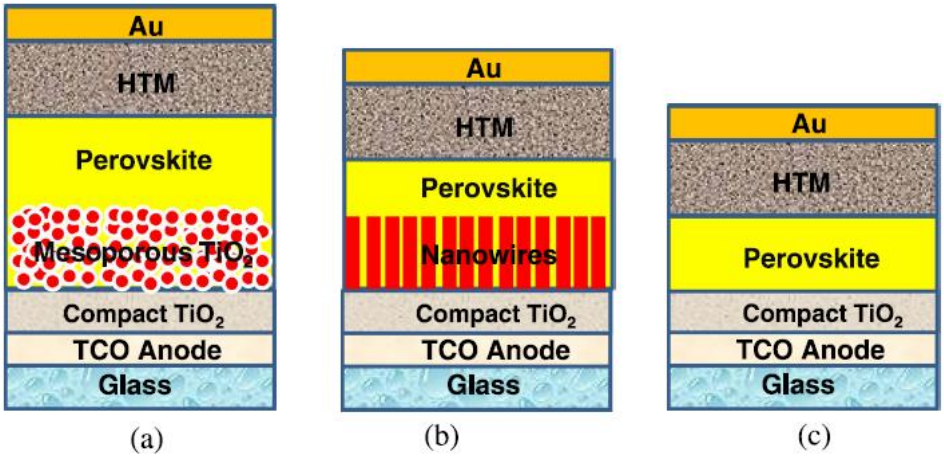

Figure 2.4: Architecture schematics of three types of photoanodes in perovskite solar cells: (a) mesoporous $TiO_2/Al_2O_3/ZrO_2$, (b) TiO_2/Zn nanowires, and (c) planar heterojunction layer. Adapted from Ref. [33]

The above configurations are popularly used in perovskite solar cell devices. Fig.2.4a,b contain a mesoporous and nanowire material which serve as scaffold (support) to the perovskite compound. In the three structures, they have in common the transparent conducting oxide (TCO) which is deposited on a glass substrate and a cathode (Au) layer which serve as the electrodes. The electron transport material, ETM (compact TiO_2) and hole transport material, HTM (spiro-OMeTAD) just like the name, extract the electrons and holes generated in the absorber layer (perovskite) and transport them to the electrodes which are in contact with the load.

2.5.2 Charge carriers in perovskite material ($CH_3NH_3PbX_3$)

The determination of charge carriers in organic-inorganic hybrid perovskite solar cells has been a challenge. This is due largely to the presence of both organic and inorganic components. This uncertainty on the nature of charge carriers transported in perovskite material has been experimentally investigated by Edri et al. [50]. It was found that the lead halide perovskite solar cells (thin film and/or inert mesoporous configuration) operate generally as p–i–n junction. A p-i-n junction has an intrinsic semiconductor material sandwiched between a p and n type extrinsic semiconductor [50]. Their study was carried out on a solar cell with mixed halide lead based perovskite, $CH_3NH_3PbI_3$ –xCl_x absorber. Figure 2.5 (c) shows the band diagram of perovskite structure. Note that, the perovskite solar cell band diagram resembles a typical p-i-n band diagram shown in fig.2.5 (b) [50]. In agreement with a previous report[50], Minemoto et

al.[49] and Tanaka et al.[51] have observed that the dominant charge carrier in lead halide perovskite is a typical Wannier- type exciton. This is similar to the type of charge carriers observed in inorganic materials [49][51]. Wannier type excitons occur when the electric field screening tends to reduce the Coulomb interaction between electrons and holes[49], [51]. The screening reduces the binding energy of the electron-hole pair and makes them move independently, unlike Frenkel excitons which occur in organic materials[49].

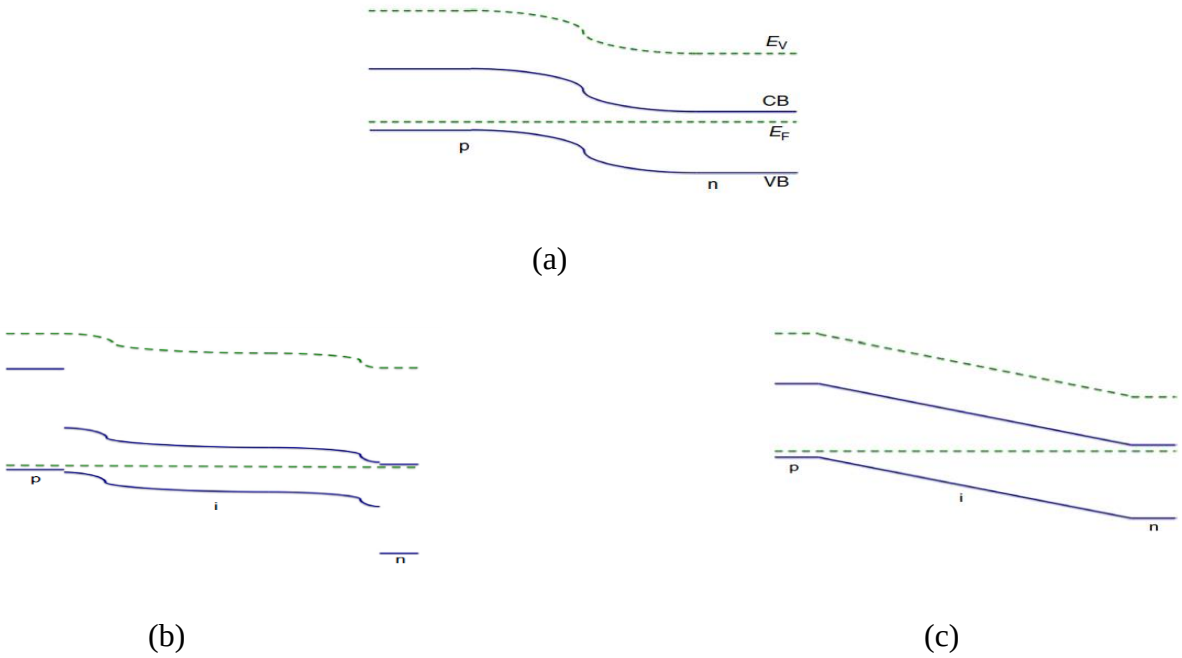

(a)

(b) (c)

Figure 2.5: A schematic band diagram of common photovoltaic devices. (a) a p–n junction solar cell. (b) A p–i–n solar cell with homogenous built-in electric field ('a-Si:H'-like). (c) perovskite-based $CH_3NH_3PbI_3$ –xClx cells. Adapted from Ref. [49].

E_v and E_f represent the vacuum and Fermi energy level while CB and VB are the conduction and valence band edge (conduction and valence band energy level).

2.5.3 Operational principle of perovskite solar cells

As discussed earlier, lead perovskite solar cells operate like p-i-n junction devices. The perovskite material serves as an intrinsic semiconductor layer, –i- while the n-type material serves as the electron transporting material (ETM) and a p-type material as the hole transporting material (HTM). A p-i-n solar cell structure is basically a p-n junction device with an undoped –i- layer sandwiched between n-type and p-type materials. The intrinsic layer, i, extends the

electric field generated in the space charge (depletion) region of the p-n junction over a wider range. The photo-generated carriers at the –i- layer are then transported towards the contacts (attached at the ends of n-type and p-type materials) by the same built-in electric field generated at depletion layer of the cell. The extension of the electric field over a wider range of the device increases the survival of the photogenerated carriers over a greater distance than those in the conventional doped semiconductor materials. The planar configuration without mesoporous structure corresponds to a p-i-n solar cell structure[38]. Such perovskite solar cells(without mesoporous scaffold) has been shown to have highest recorded efficiency of 19.3% [21]. This suggests shows that the mesoporous perovskite solar cell structure is not a prerequisite for obtaining a better performing solar cell device.

2.6 Excitons

Excitons are fundamental quantum of electronic excitation consisting of a negatively charged electron and a positively charged hole bound to each other by electrostatic attraction. They are created when a solid absorbs photons.

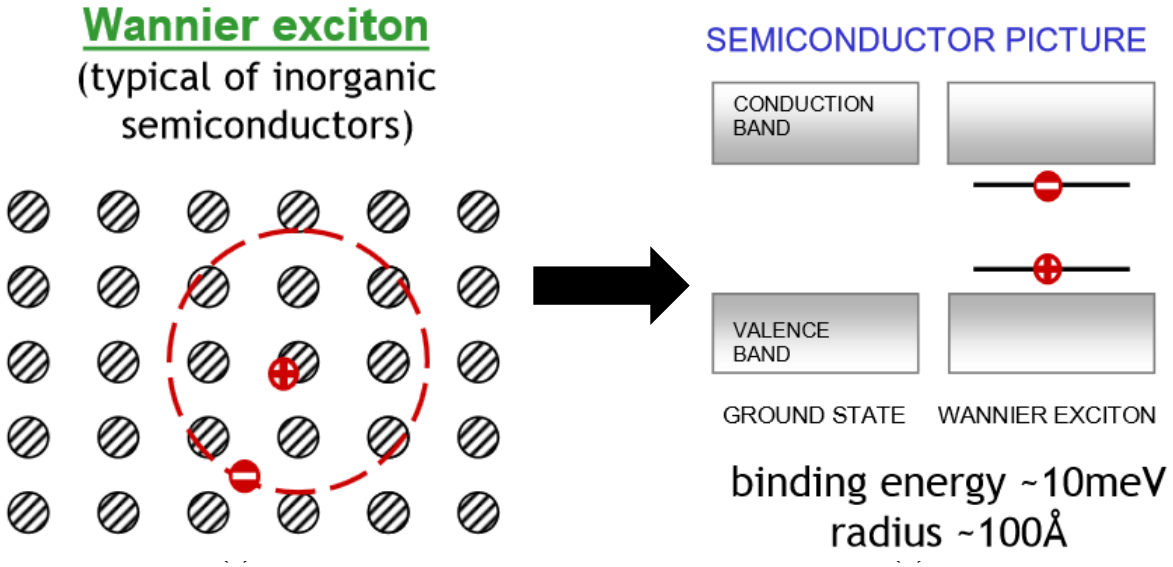

Figure 2.6: (a) Diagram of Wannier-type exciton (b) Band diagram of a semiconductor material. Adapted from Ref.[59]

Excitons are of two types, the Wannier excitons (fig. 2.6a) and Frenkel excitons (fig.2.7a), based on their size relative to the interatomic or intermolecular distances in the material.

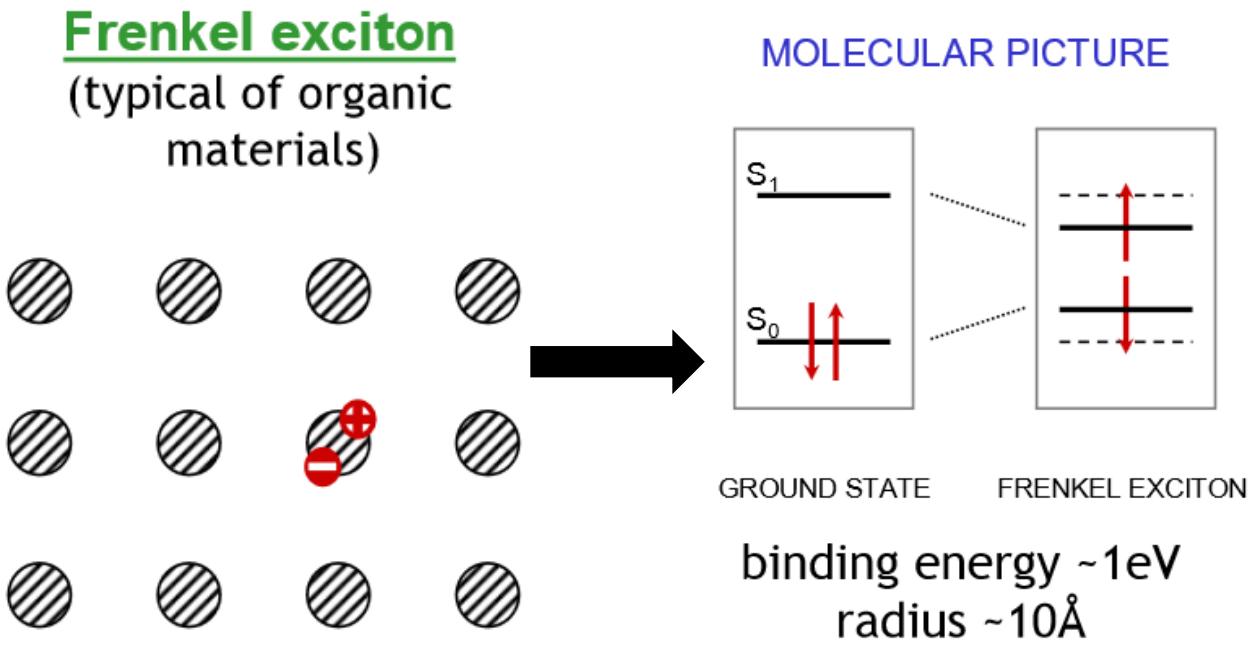

(a) (b)

Figure 2.7: (a) Diagram of Frankel-type exciton (b) Molecular band diagram of an organic material. Adapted from Ref. [59]

In Wannier excitons, typically observed in covalent semiconductors and insulators, the electron and hole are separated by a distance much larger than the atomic spacing, so that the effect of the crystal lattice on the exciton is negligible. In Frenkel excitons, are mostly found in organic materials eg. molecular or rare-gas crystals, the electron and hole are separated by a distance comparable to the atomic spacing, so that the exciton is localized to a single site at any given time. Wannier excitons move essentially like free particles, while motion of Frenkel excitons is seen as hopping from one site to another[52].

CHAPTER THREE

NUMERICAL SIMULATION

3.1 INTRODUCTION

Computational simulation is a technique of studying and analyzing the behavior of a real device or an imaginary system by mimicking it with a computer application. A simulation is based on a mathematical model that describes the system.

Numerical simulation technique of solar cells devices has over the years proven to be a viable tool for studying and understanding the properties of solar cell devices such as the optical, electrical and mechanical properties of complex solar cell devices[53]. It also helps to reduce processing cost and time spent on solar cell device fabrication by providing useful information on how to vary the production parameters to improve the device performance [49] .

In this section, we shall first describe the operation of Solar Cells Capacitance Simulator (SCAPS), which was used to carry out the simulations. We will then derive the mathematical equations which are solved by the software. Furthermore, device simulation and optimization will be carried out using the device structure that shall be described.

3.2 Description of working principles of SCAPS

The SCAPS 1D simulator was developed by Burgelman et. al. to simulate the electrical characteristics of thin-film heterojunction solar cells by solving the basic semiconductor device equations under steady state conditions Ref.[26]. It was used in this work to explore the real device ($MASnI_3$) solar cell with material parameters modified for better performance. The software allows for the inclusion of deep bulk level and interface defect recombination (non-radiative recombination). Some of the recombination losses prevalent in the device under consideration are radiative recombination (ie. direct band-to-band recombination) and interface recombination which is accounted for by the Shockley-Read-Hall recombination (propagated by defects or traps). The flow chart below shows step-by-step stages in running a simulation with SCAPS.

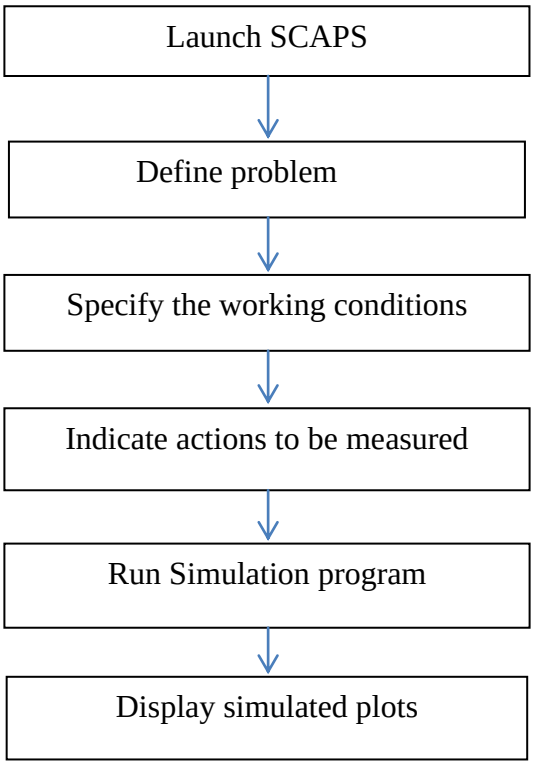

Figure 3.1: Simulation procedure

3.3 Derivation of the governing equations in SCAPS

The simulation is based on the solution of three governing semiconductor equations: Poisson's equation, electron and hole continuity equations. SCAPS numerically solves these three coupled partial differential equations for the electrostatic potententials electron and hole concentration as function of positions x.

3.3.1 Poisson equation

The Poisson equation connects the electric potential Φ and the charge:

$$\frac{d}{dx}\left(-\varepsilon(x)\frac{d\Phi}{dx}\right) = q[p(x) - n(x) + N_D^+(x) - N_A^-(x) + p_t(x) - n_t(x)] \qquad (3.1)$$

where p is the free hole density, n is the free electron density, $N_D^+(x)$ is the ionized-donor density, $N_A^-(x)$ is the ionized-acceptor density, $n_t(x)$ and $p_t(x)$ are trapped electron density and trapped hole density respectively, and ε is the dielectric constant of the medium.

SCAPS determines the following unknown variables in a solar cell simulation, the electrical potential Φ and the carrier concentrations p and n (Φ, n, p) Ref.[26] by solving the coupled differential equations.

3.3.2 Continuity equations

Another equation SCAPS solves is the continuity equation. Every action undergone by charge carriers in a semiconductor device gives rise to a change in the carrier concentration with time Ref.[54]. These equations are in two folds, the electrons and the holes equations. The derivation of the continuity equation is given below.

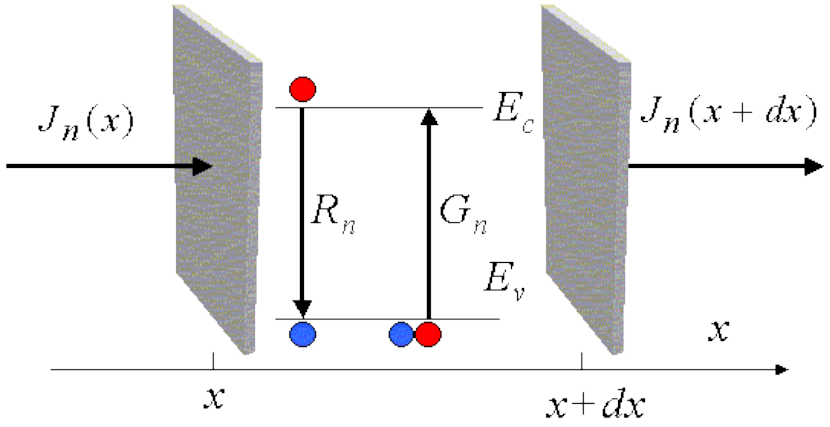

Figure 3.2: Electron currents and possible recombination and generation processes [Van Zeghbroeck, 2011]

The figure above shows an elemental volume in which a one- dimensional electron flux $J_n(x)$ and $J_n(x+dx)$ entering and leaving the elemental volume at x and $x+dx$ repectively. R_n and G_n are respectively rates of electron recombination and generation in the semiconductor device. If $-qn(x,t)$ is the electron carrier density in the volume.

Then, the total carrier charge in the volume $= -qn(x,t)dV = -qn(x,t)dxdydz = -qn(x,t)A_x dx$

Total number of charges generated $= -qG_n dV = -qG_n A_x dx$

Total number of charges recombined $= -qR_n dV = -qR_n A_x dx$

By conservation law, the change of charges in the volume = Rate of (inflow-outflow) of charges + Rate of (Generation-Recombination) of charges in the volume.

$$-q\frac{\partial n(x,t)}{\partial t}A_x dx = [J_n(x) - J_n(x+dx)]A_x - q(G_n - R_n)A_x dx \quad (3.2)$$

By Taylor expansion, $J_n(x+dx) \sim J_n(x) + \frac{\partial J_n}{\partial x}dx$

$$\Rightarrow -q\frac{\partial n(x,t)}{\partial t}A_x dx = \left[J_n(x) - J_n(x) - \frac{\partial J_n}{\partial x}dx\right]A_x - q(G_n - R_n)A_x dx$$

$$-q\frac{\partial n(x,t)}{\partial t}A_x dx = -\frac{\partial J_n}{\partial x}A_x dx - q(G_n - R_n)A_x dx \quad (3.3)$$

Dividing through eq. (3.3) by $-qA_x dx$

$$\frac{\partial n(x,t)}{\partial t} = \frac{1}{q}\frac{\partial J_n}{\partial x} + G_n(x,t) - R_n(x,t) \quad (3.4)$$

Similarly for holes we have,

$$\frac{\partial p(x,t)}{\partial t} = -\frac{1}{q}\frac{\partial J_p}{\partial x} + G_p(x,t) - R_p(x,t) \quad (3.5)$$

Equations (3.4) and (3.5) are 1-D continuity equation for electrons and holes respectively.

3.3.3 Carrier transport equations

There are two main carrier transport mechanisms in semiconductor devices which are Drift and Diffusion. This movement of charge carriers generates current in the device. We shall derive the current density expressions for these carriers.

a) Drift current density

Drift current is the current generated by the movement of charge carriers due to an applied electric field, E as shown in fig.3.3 below.

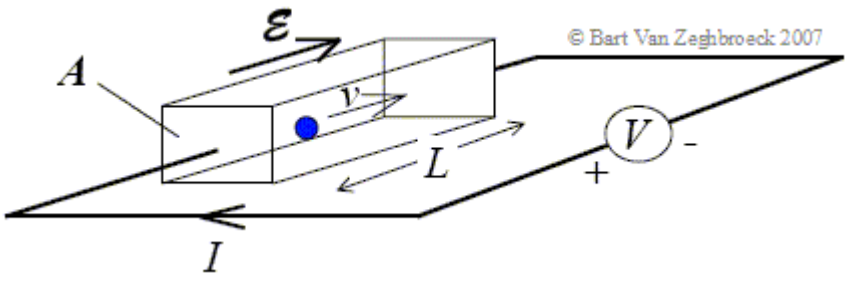

Figure 3.3: Drift of a carrier due to an applied electric field

Where J = current density, σ = conductivity of the material, E= applied electric field.

When an E- field **E** is applied to a semiconductor device, it produces a force, **F** on the charge carriers (say electron) which will experience a net acceleration**, a** Ref. [55].

$$\boldsymbol{F} = m_e^* \boldsymbol{a} = -q\boldsymbol{E} \tag{3.6}$$

$$-q\boldsymbol{E} = \frac{m_e^* \boldsymbol{v_d}}{t}$$

$$\boldsymbol{v_d} = -\frac{qt\boldsymbol{E}}{m_e^*} = -\mu_n \boldsymbol{E}$$

$$\boldsymbol{v_d} = -\mu_n \boldsymbol{E} \tag{3.7}$$

Where, $\boldsymbol{v_d}$ is the drift velocity, q is the electron charge, $\mu_n = \frac{qt}{m_e^*}$ is the electron mobility, t is time and m_e^* is the effective mass of electron.

Considering fig. 3.3, the total current flux J passing through the box of volume V with length L is the total number N of charges passing through a unit area A per unit time.

Mathematically

$$J_{n|drift} = -\frac{NqL}{At} = -\frac{Nq\boldsymbol{v_d}}{A}$$

$$J_{n|drift} = -nq(-\mu_n \boldsymbol{E})$$

n is electron number density given as $\frac{N}{V}$. If we are considering the electron passing through the entire volume of the box $\frac{N}{A} = \frac{N}{V}$

$$J_{n|drift} = nq\mu_n \boldsymbol{E} \tag{3.8}$$

Similarly for holes the current density becomes

$$J_{p|drift} = pq\mu_p \boldsymbol{E} \tag{3.9}$$

So the total drifts current becomes $J_{drift} = J_{n|drift} + J_{p|drift}$

$$J_{drift} = q\boldsymbol{E}(n\mu_n + p\mu_p)$$

b) Diffusion current density

Diffusion is defined as the movement of particles from a region of higher concentration to a region of lower concentration. We consider here, a thermal equilibrium state of the system where the net flow of electrons and holes do not significantly alter the thermal equilibrium condition of the system Ref.[55]. Fig.(3.5) shows the electron concentration variation with position x in 1-D assuming uniform temperature so that the thermal velocity of the electron is independent of x.

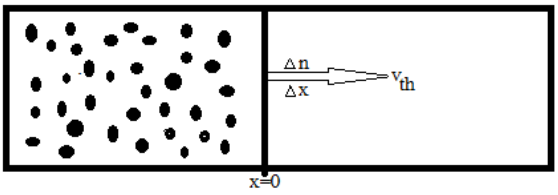

Figure 3.4: Representation of diffusion process

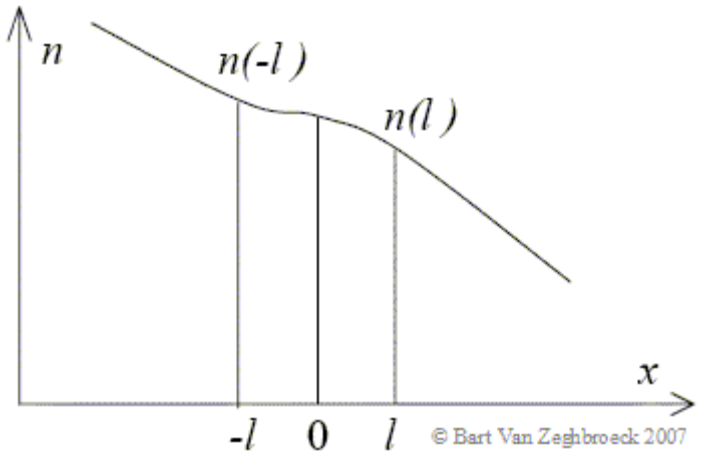

Figure 3.5: Carrier density profile used to derive the diffusion current expression

To calculate diffusion current for electron, we start by defining some parameters

l = mean free path of carrier

$n(x)$ = carrier concentration

v_{th} = thermal velocity

Flux = concentration × velocity

The flux of carrier crossing $x = 0$ from a distance $x = -l$ from left to right is

$$F_{l-R} = \frac{1}{2} n(x = -l) v_{th} \tag{3.10}$$

The carrier flux crossing $x = 0$ from a distance $x = \ l$ from right to left is

$$F_{R-l} = \frac{1}{2} n(x = l) v_{th} \tag{3.11}$$

The factor $\frac{1}{2}$ is because we considered a half path travel of the carrier flow to the right while the other half to the left.

The net flux of carriers crossing $x = 0$ from left to right is

$$F_n = F_{l-R} - F_{R-l} = \frac{1}{2}[n(-l) - n(l)]v_{th} \quad (3.12)$$

Taylor expanding the carrier concentration about $x = 0$

$$n(-l) = n(0) - l\frac{dn}{dx} \quad (3.13)$$

$$n(l) = n(0) + l\frac{dn}{dx} \quad (3.14)$$

Substituting eqs. (3.13), (3.14) into (3.12)

$$F_n = \frac{1}{2}\left[n(0) - l\frac{dn}{dx} - n(0) - l\frac{dn}{dx}\right]v_{th} = -lv_{th}\frac{dn}{dx}$$

$$F_n = -D_n\frac{dn}{dx} \quad (3.15)$$

$D_n = lv_{th}$

The electron diffusion current density $J_{n|diff} = -qF_n$

Therefore

$$J_{n|diff} = qD_n\frac{dn}{dx} \quad (3.16)$$

Similarly, for holes

$$J_{p|diff} = -qD_p\frac{dp}{dx} \quad (3.17)$$

The diffusion current for both electrons and holes is thus given as;

$J_{diff} = J_{n|diff} + J_{p|diff}$

$$J_{diff} = q\left(D_n\frac{dn}{dx} - D_p\frac{dp}{dx}\right)$$

c) Total current density, J

Generally, the total electron current density J_n for both drift and diffusion is:

$$J_n = J_{n|drift} + J_{n|diff}$$

$$\Rightarrow \quad J_n = q\left(n\mu_n \boldsymbol{E} + D_n \frac{dn}{dx}\right) \tag{3.18}$$

Similarly, $J_p = J_{p|drift} + J_{p|diffusion}$

$$\Rightarrow \quad J_p = q\left(p\mu_p \boldsymbol{E} - D_p \frac{dp}{dx}\right) \tag{3.19}$$

Where D_n and D_p are the diffusivity which can be determined by Einstein relation given as:

$$D_n = \frac{\mu_n K_B T}{q}$$

$$D_p = \frac{\mu_p K_B T}{q}$$

Finally, eqs.(3.18) and (3.19) are the carrier current transport equation for electrons and holes, respectively, of a 1D semiconductor device.

Table 3.1: Summary of the basic device equations

Poisson equation	$\frac{d}{dx}\left(-\varepsilon(x)\frac{d\Phi}{dx}\right) = q[p(x) - n(x) + N_D^+(x) - N_A^-(x) + p_t(x) - n_t(x)]$
Continuity equation for electrons	$\frac{\partial n(x,t)}{\partial t} = \frac{1}{q}\frac{\partial J_n}{\partial x} + G_n(x,t) - R_n(x,t)$
Continuity equation for holes	$\frac{\partial p(x,t)}{\partial t} = -\frac{1}{q}\frac{\partial J_p}{\partial x} + G_p(x,t) - R_p(x,t)$
Current density equation for electrons	$J_n = q\left(n\mu_n \boldsymbol{E} + D_n \frac{dn}{dx}\right)$

Current density equation for holes	$J_p = q\left(p\mu_p \boldsymbol{E} - D_p \frac{dp}{dx}\right)$

Under steady state, $\frac{\partial n}{\partial t}$ = 0 so that the continuity equations become

$$\frac{1}{q}\frac{\partial J_n}{\partial x} + G_n(x) - R_n(x) = 0$$

Substituting J_n from eq. 3.18 into the equation above, we obtain

$$n\mu_n \frac{dE}{dx} + \mu_n E \frac{dn}{dx} + D_n \frac{d^2n}{dx^2} + G_n(x) - R_n(x) = 0$$

Similarly for holes

$$-p\mu_p \frac{dE}{dx} - \mu_p E \frac{dp}{dx} + D_p \frac{d^2p}{dx^2} + G_p(x) - R_p(x) = 0$$

3.4 Generation (Gn, Gp) and recombination (Rn, Rp)

Generation and Recombination are two opposite processes that occur in semiconductor devices. While generation describes the process whereby electrons and holes are created, recombination is the process whereby they are annihilated or destroyed. When a semiconductor is disturbed from equilibrium state, the electrons and holes concentrations change from their equilibrium value[27]. In order to restore the system to its equilibrium condition, recombination-generation (R-G) processes occur to eliminate or stabilized excess or deficit carrier respectively. These R-G processes occur in so many ways, which are: Direct band-to-band generation or recombination, indirect R-G rcombination or recombination by trap centers.

R-G processes result in the change of the carrier concentration which indirectly affects current flow in semiconductor by controlling the concentrations of carriers that are involved in current transport processes.

3.5 Absorption Coefficient α

The absorption coefficient determines how far into a material light of a particular wavelength can penetrate before it is absorbed. In a material with a low absorption coefficient, light is only poorly absorbed, and if the material is thin enough, it will appear transparent to that wavelength. The absorption coefficient depends on the material and also on the wavelength or photon energy of light which is being absorbed. Semiconductor materials have a sharp edge in their absorption coefficient, since light which has energy below the band gap does not have sufficient energy to excite an electron into the conduction band from the valence band. Consequently this light is not absorbed. The absorption coefficient is expressed as Ref. [56]:

$$\alpha = A\left(h\upsilon - E_g\right)^{1/2}$$

Where A is the absorption constant, $h\upsilon$ is the photon energy and E_g is the bandgap of the semiconductor.

3.6 Real device analysis

The real device of this work which was reported by Noel et al. [25] was based on the mesoporous structure as shown below. The mesoporous structure serves as a scaffold for the perovskite absorber. In this device a colloidal solution of TiO_2 which was deposited by spin coating was used with a thickness of 400nm.

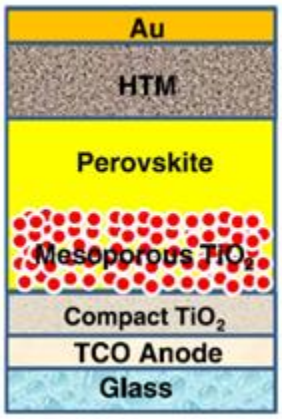

Figure 3.6: Mesoporous architecture of real device

The minority carrier diffusion length and lifetime were experimentally determined to be 30nm and ~0.2ns, respectively, which are low compared to those of its Pb counterpart and, thus requires careful design engineering for efficient extraction of charge carriers before recombination[27]. A band-to- band recombination was reported experimentally with a radiative recombination coefficient $\Upsilon = 1.4 \times 10^{-9} cm^3/s$. The perovskite was found to be a p-type material due to the oxidation of Sn^{2+} to Sn^{4+} which acts as a p-type semiconductor with a high doping concentration of about 6×10^{18}.

3.5 Simulation Device Structure

The simulation of tin-based perovskite solar cell was based on the n-i-p configuration which can be simulated using any thin-film simulator and therefore considered similar to the structure of thin film semiconductor based solar cell. To achieve this n-i-p configuration, a real designed was re-structured to match the n-i-p junction. Figures 3.7(a) and (b) are the junction configuration of the real and the simulated devices. Thus, the new structure is considered as a planar heterojunction.

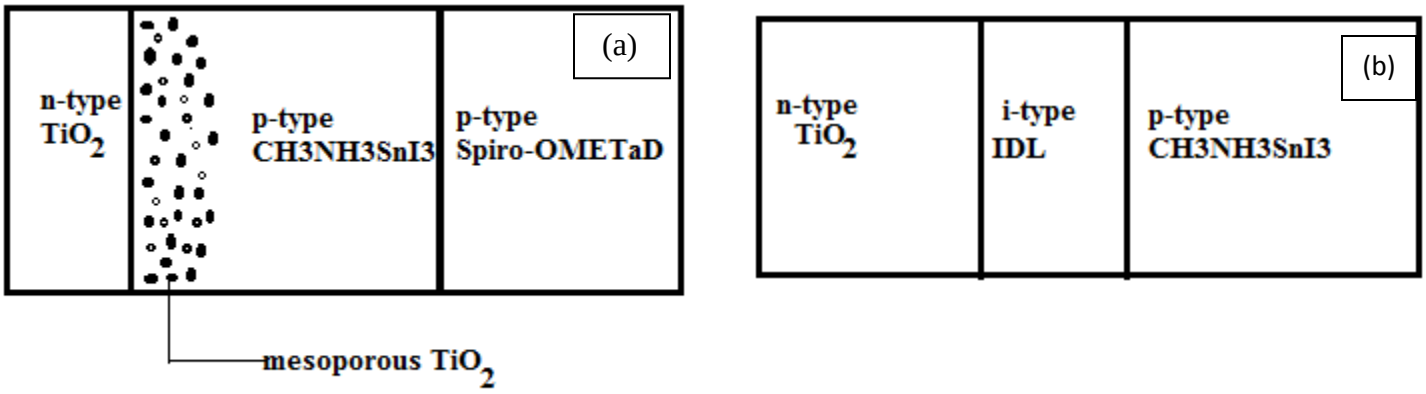

Figure 3.7: (a) p-n junction of real device (b) p-i-n junction of simulated device

This new configuration was based on the fact that organic and inorganic perovskites can also serve as hole transport material (HTM) as well as an absorber in perovskite solar cells[41] thereby reducing the cost of device fabrication. The intrinsic layer –i- is a very thin layer which has properties between the TiO_2 and $CH_3NH_3SnI_3$. This intrinsic interface layer takes into account interface defect recombination. The defect density N_t at the interface was calculated by the formula

$$N_t = \frac{1}{\sigma v_{th} \tau}$$

Where σ is the capture cross section which was set as 1×10^{-13}cm^2, v_{th} is the thermal velocity of the absorber ($3 \times 10^{-7} cm^2/s$) and τ is the lifetime of minority carrier.

Table 3.2 shows the values of the most useful cell parameters required for the simulation. These values were chosen on the basis of theoretical considerations, experimental data and existing literature or in some cases, reasonable estimates. Most of the parameters used for the absorber and the thicknesses of the other layers were extracted from the literature [25] while the parameters for other layers in the Table were gotten from the works reported by [57] and [49]. The remaining parameters were estimated or calculated, though the most important parameters (E_g, ε_r, χ, μ_n, μ_p etc) for the simulation were obtained from literature. The work function of the cathode electrode (Au) is -5.1eV which serves as back contact for holes transport.

Table 3:2 Device simulation parameters

Parameters	SnO_2:F(TCO)	TiO_2 (ETM)	Interface layer	CH3NH3SnI3 (absorber)
Thickness, x (µm)	0.5	0.05	0.048	0.4
Bandgap, E_g (eV)	3.5	3.2	2.22	1.23
Electron affinity, χ (eV)	4.4	4.26	4.22	4.17
Dielectric ratio, $\varepsilon/\varepsilon o$	9.0	50	27.5	10
Density of states, N_c (cm^{-3})	2.2×10^{18}	1.0×10^{21}	1.5×10^{20}	2.1×10^{18}
Density of states, N_v (cm^{-3})	1.8×10^{19}	2.0×10^{20}	1×10^{20}	1.9×10^{18}
Elect. mobility,μ_n(cm^2/Vs)	20.0	0.006	0.8	1.6
Hole mobility, μ_p (cm^2/Vs)	10.0	0.006	0.1	0.2
Defect density,N_t (cm^{-3})	….	….	2.5×10^{15}	.....
Thermal velocity of electron (cm/s)	10^7	10^7	2.0×10^7	3.0×10^7
Thermal velocity of hole (cm/s)	10^7	10^7	2.0×10^7	3.0×10^7
N_A (cm^{-3})	….	5×10^{19}	2.8×10^{19}	6.0×10^{18}
N_D (cm^{-3})	2×10^{19}	….	2.8×10^{19}	.....

The absorption profile in fig.3.8 is as adopted from experiment in which the absorption constant used in this simulation was extracted from. As discussed earlier that the absorption edge of tin-perovskite ~1000nm i.e. it can absorb solar radiation close to that in the solar spectrum.

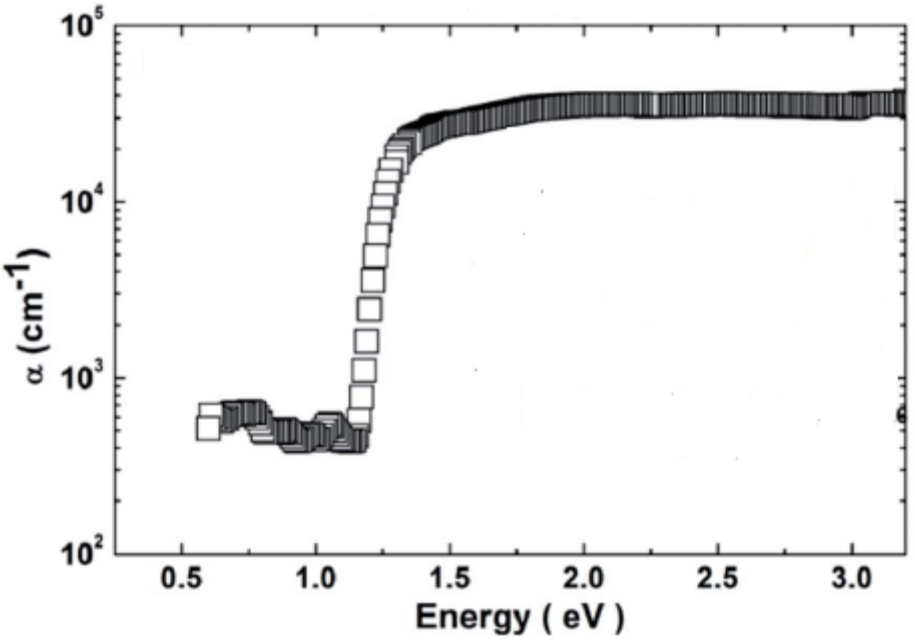

Figure 3.8: The absorption profile of CH3NH3SnI3. Adapted from Ref.[25]

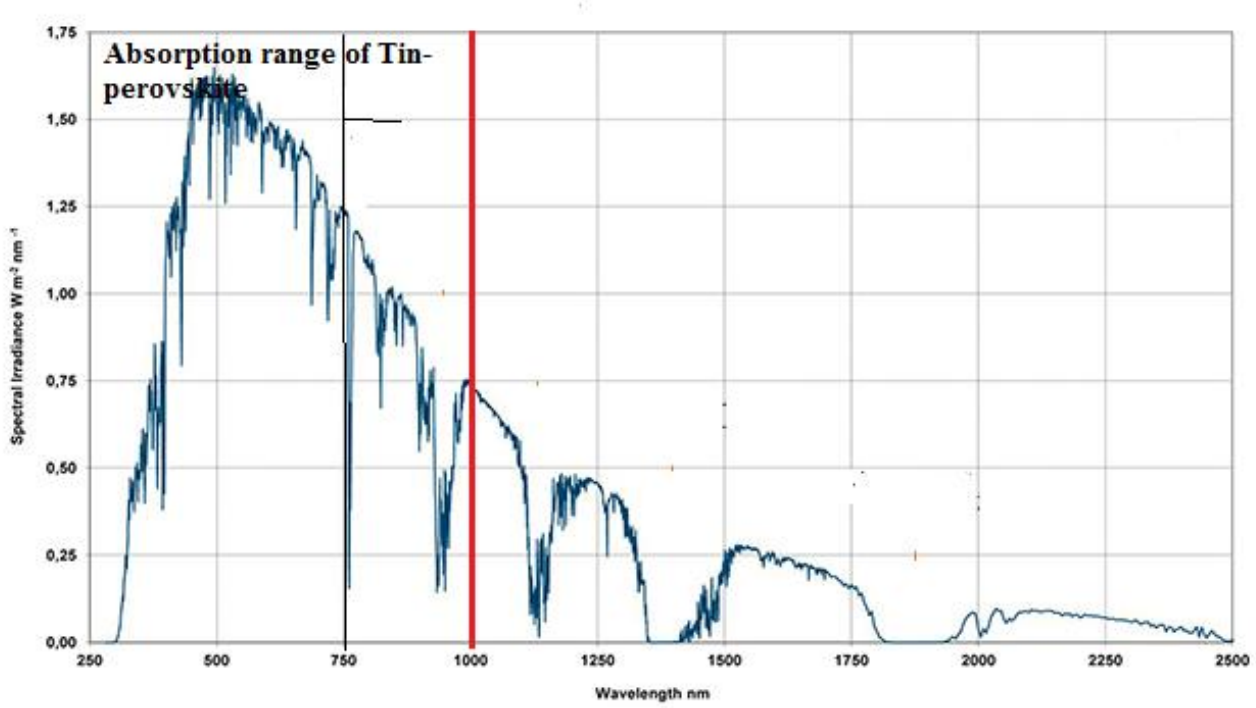

Figure 3.9: solar irradiance spectrum of AM1.5

The red line in fig. 3.9 shows the range of solar radiation absorption of $MASnI_3$ which shows absorption over the visible region and close to near infrared**.**

CHAPTER FOUR

RESULT AND DISCUSSION

This chapter discusses the results obtained from the numerical simulations. The changes in the cell performance that happen in the variation of cell parameters are discussed. The parameters investigated are the hole density in the absorber and the thickness of the absorber.

4.1 Device characterization

Figure 4.1(a) and (b) show the material layers and the band diagram of the device respectively. Light enters the cell through the transparent conductive oxide layer (TCO), passes through the compact electron transporting layer, the defect layer which is partly an absorber and enters the absorber which also double as the hole transport material.

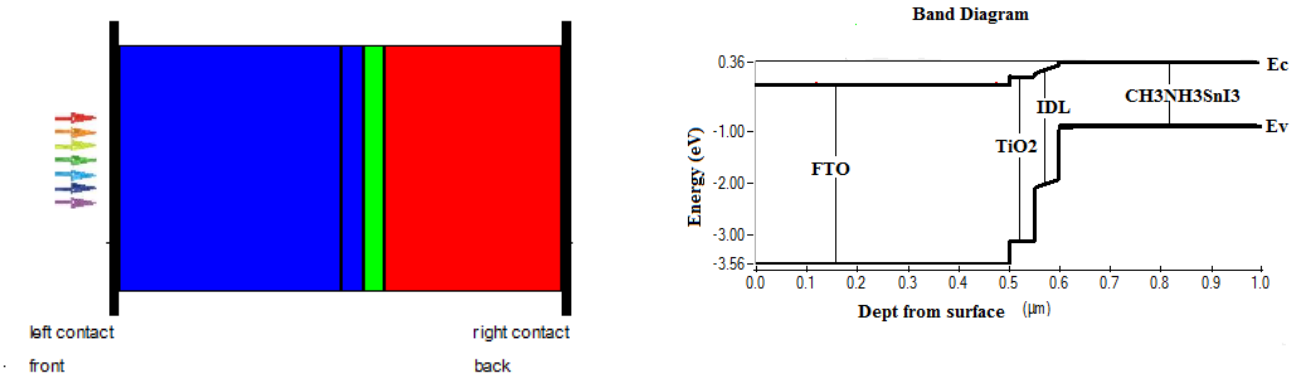

(a) (b)

Figure 4.1: (a) Simulated solar cell structure (b) Energy band diagram

4.2 J-V curve of n-i-p device

The J-V characteristic curve obtained by simulating with the data in Table 3 is shown in Fig. 4.3(a) with the output cell parameters V_{oc} = 0.90V, J_{sc} = 16.85mA/cm^2, FF = 42.15%, and PCE(η) = 6.41% under AM1.5 simulated sunlight of 100mW/cm^2. These values are similar to the experimental values from Ref.[25]: literature as V_{oc} = 0.88V, J_{sc} = 16.8mA/cm2, FF = 0.42, η = 6.4%. This result confirms our new configuration as equivalent to the real device structure.

Simulating with the data in the table 3 resulted in the J-V curve in fig. 4.2(a) with negligible difference with that that of experiment in fig. 4.2(b).

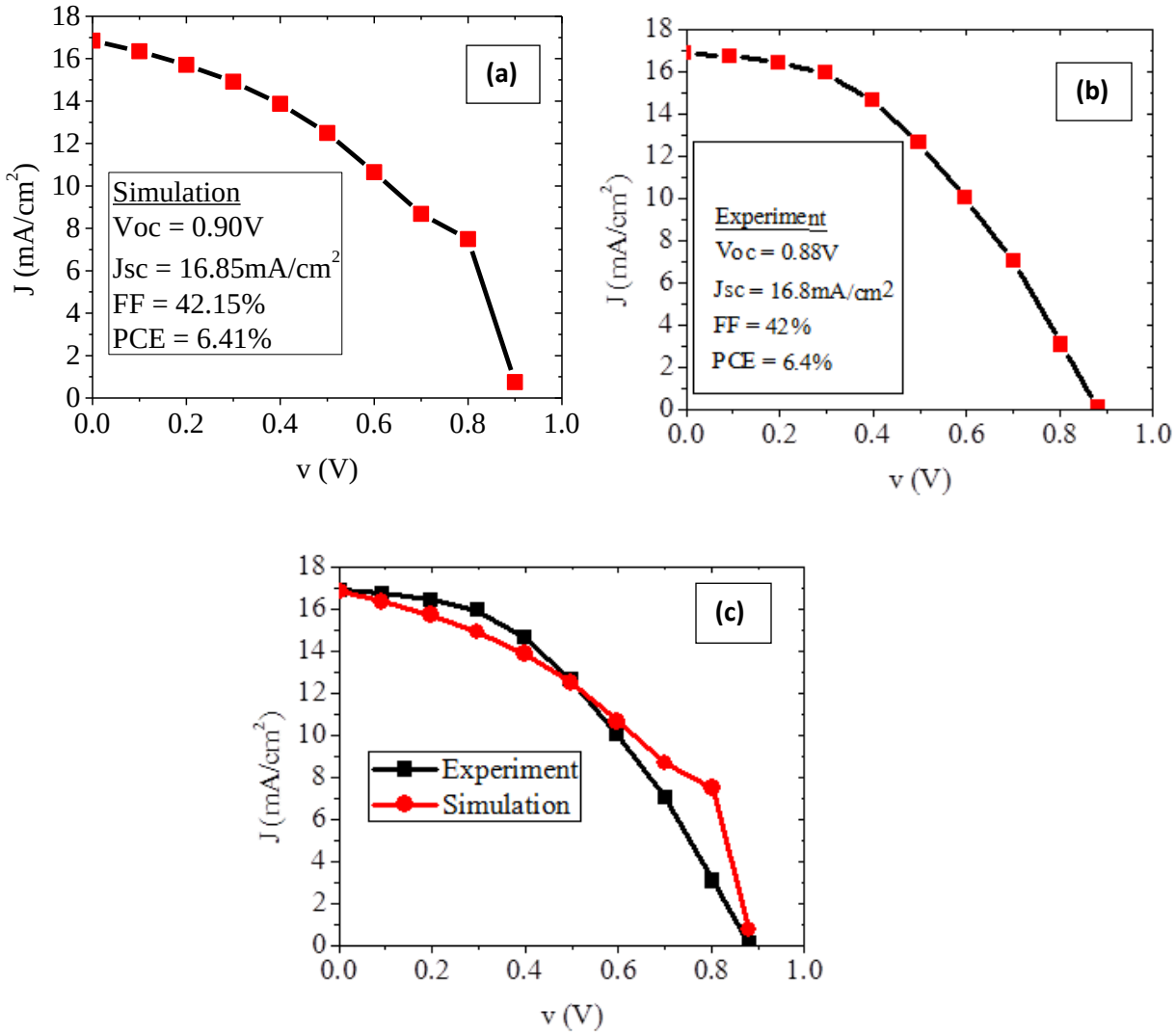

Figure 4.2: (a) Simulated J-V curve (b) Experimental J-V curve (c) Simulated and experimental J-V characteristics curves

To determine the effect of interface defect recombination, a check was carried out by removing the interface layer which accounts for both interface defect recombination which is an extension of Schockley-Read- Hall recombination Ref.[58]. The J-V curve obtained by this check is as shown in Fig.4.3 with a higher efficiency of 8.17% compared to the previous set-up. This increase in PCE is as a result of increase in V_{oc} which is affected by recombination on defect, validating the report by[57].

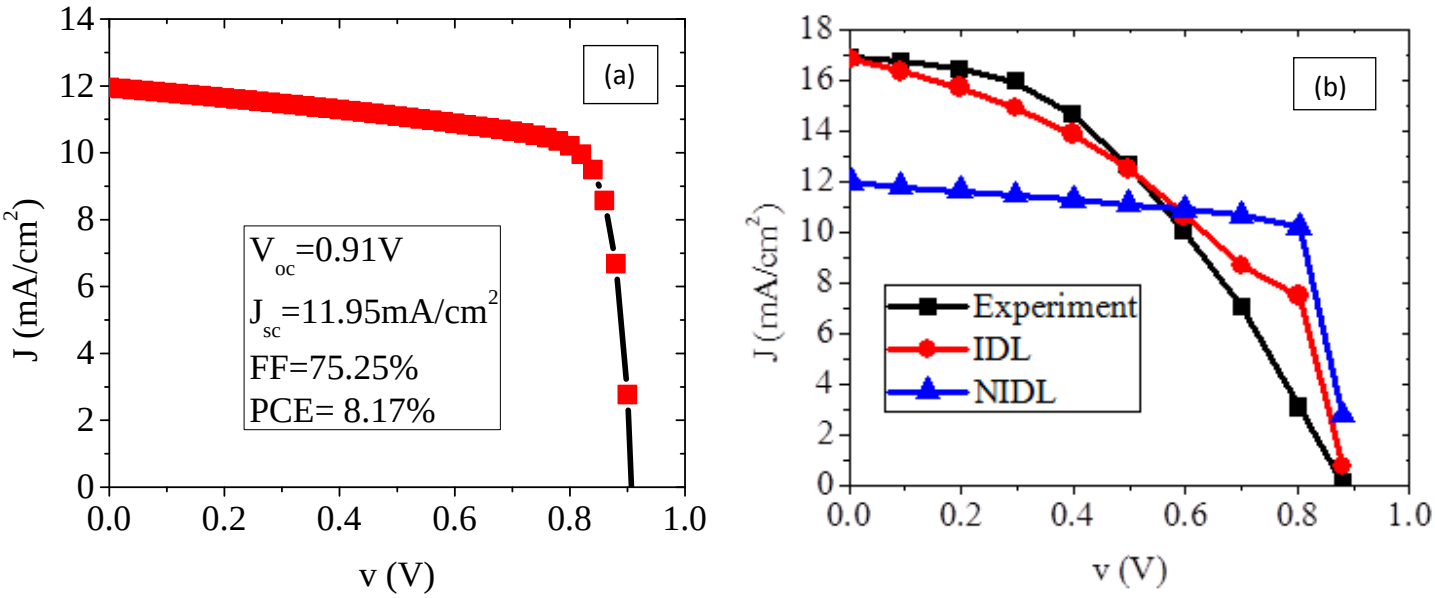

Figure 4.3: (a) J-V curve of the photovoltaic structure without an interface layer (b) J-V curve plot of both the experiment and simulated p-i-n and p-n junction.

4.3 Effect of doping concentration of the absorber on the simulated device

The high doping acceptor concentration N_A ranging from 10^{16} to 10^{19} cm^{-3} as reported by[25], [28] due to due the Sn^{4+} impurity is an impediment to achieving long diffusion length in tin iodide perovskite. This also contributes to the low performance of tin iodide perovskite solar cells. We performed device simulations for this system at different values of N_A. The resulting J-V characteristics are shown in Fig. 4.4(a). The results are summarized in Table 4.1, from these results, we observe that there is a decrease in device performance (η) as doping concentration increases. Increased doping concentration, increases recombination and reduces the lifetime of carrier according, see Ref.[25].

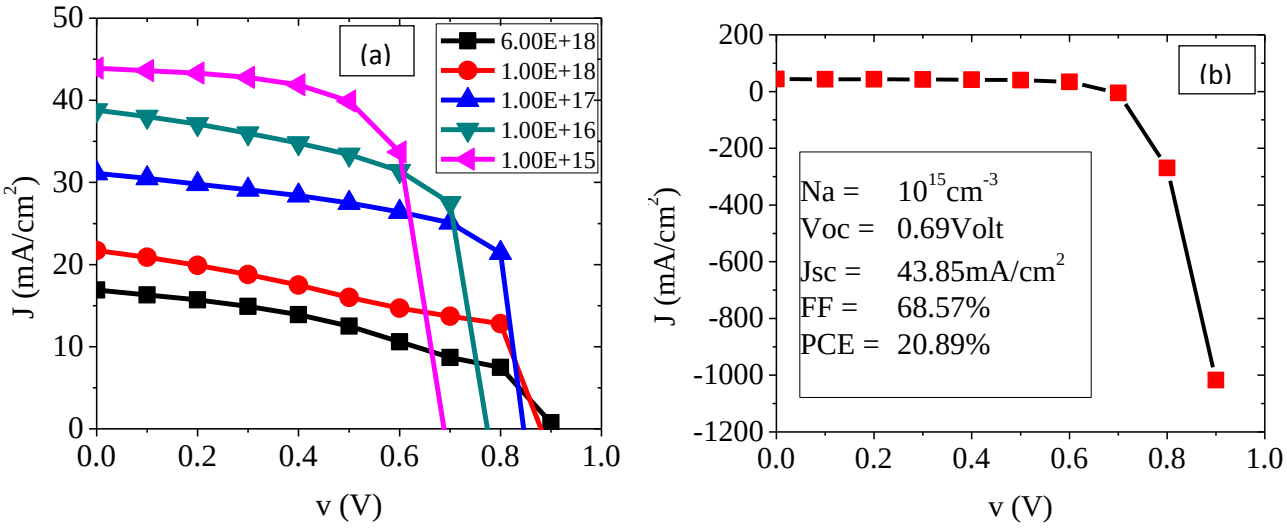

Figure 4.4: (a) J-V characteristics for the $MASnI_3$ cell at different acceptor concentration N_A in cm^{-3} (b) A J-V curve and device parameters for the lowest acceptor concentration ($N_A=10^{15}cm^{-3}$) in this work.

Table 4.1: Variation of doping concentration with device parameters

N_A (cm^{-3})	V_{oc} (V)	J_{sc} (mA/cm^2)	FF (%)	η (%)
10^{18}	0.89	21.66	51.70	9.99
10^{17}	0.87	31.11	66.63	18.03
10^{16}	0.79	38.81	63.90	19.581
10^{15}	0.69	43.65	68.57	20.89

4.4 Effect of the absorber thickness on the device parameters

The plots below show the thickness variation from (0.2-1) μm of the absorber against the performance parameters of the device. Fig. 4.5(a) shows constant V_{oc} against various thicknesses. Fig.4.5(b),(c),(d) show an increase in J_{sc}, V_{oc}, PCE (η) with thickness with an optimum thickness of 0.7 μm and a sharp decrease in value after the optimum thickness.

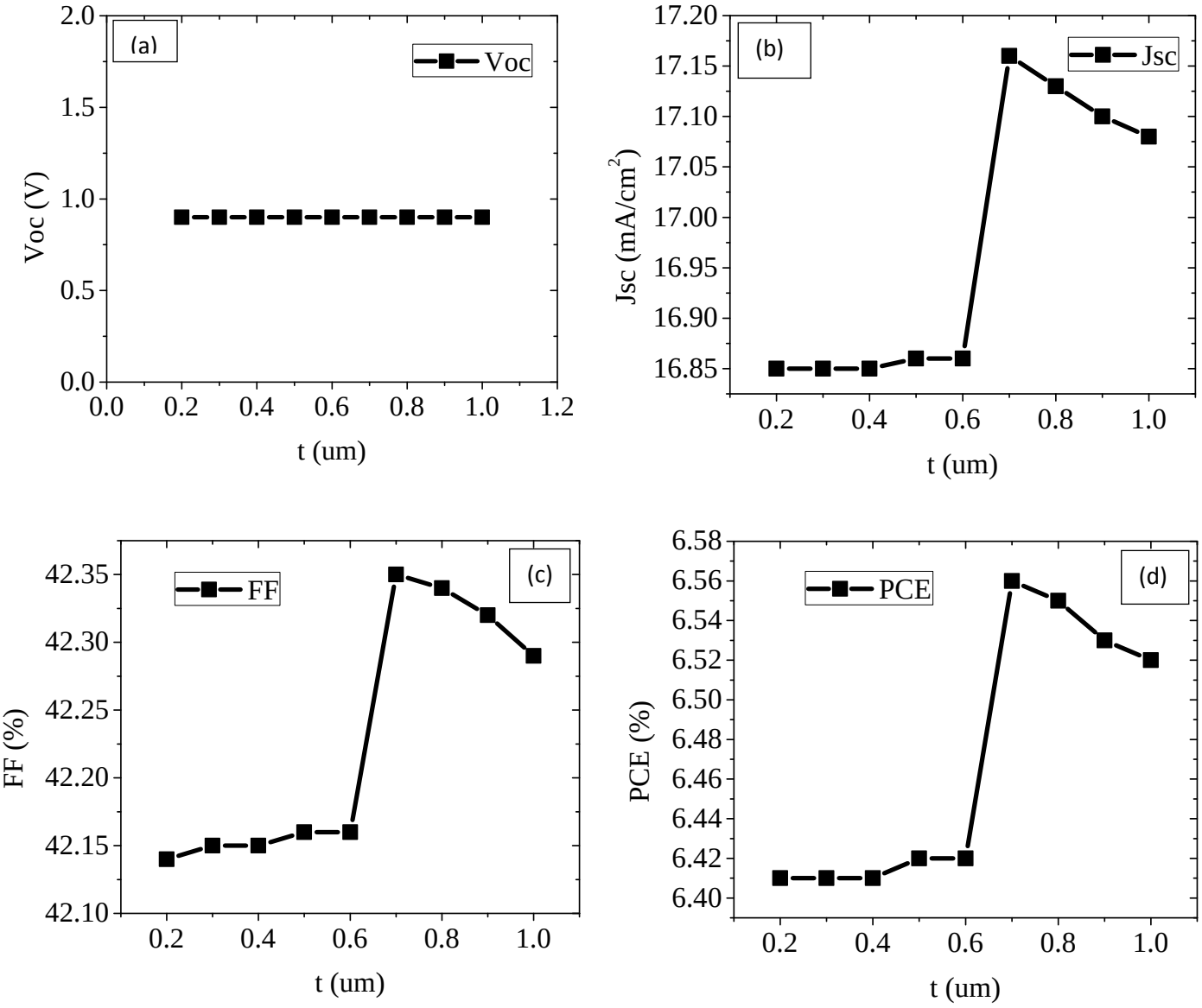

Figure 4.5: variation of the absorber thickness with the device parameters (Voc,Jsc,FF and PCE)

Table 4.2: Variation of absorber thickness with device parameters

Thickness(μm)	V_{oc}(V)	J_{sc}(mA/cm^2)	FF(%)	η(%)
0.2	0.9	16.85	42.14	6.41
0.3	0.9	16.85	42.15	6.41
0.4	0.9	16.85	42.15	6.41
0.5	0.9	16.86	42.16	6.42
0.6	0.9	16.86	42.16	6.42
0.7	0.9	17.16	42.35	6.56
0.8	0.9	17.13	42.34	6.55
0.9	0.9	17.1	42.32	6.53
1	0.9	17.08	42.29	6.52

CHAPTER FIVE

CONCLUSION AND RECOMMENDATION

5.1 CONCLUSION

In conclusion, it has been observed from the results discussed in chapter four that solar cells with tin iodide perovskite as the absorber can perform excellently well like at low (~$10^{15}cm^{-3}$) doping concentrations its lead counterpart. An efficiency of >18% should be achievable with tin-based perovskite by preparing the device in an air tight condition in order to reduce oxidation of Sn. The planar configuration proposed in this work was to enable the simulation with SCAPS. Solar cells with tin-based perovskites are not toxic unlike the lead based ones and at the same time, with careful engineering should be able to obtain similarly high efficiencies.

5.2 RECOMMENDATION

Further work, experimental and numerical, should be done on this area of perovskite as has been done for lead-based perovskite. An anti-oxidant material can also be incorporated into the anti-reflective coating to reduce further oxidation of Sn^{2+} to Sn^{4+} in the tin-iodide perovskite solar cells. Experimentalists can also investigate the use of mixed halides in the tin halide perovskites based devices as a possible means to increasing the cell performance as observed in the lead-based perovskite cells.

REFERENCES

[1] Stone, “photovoltaics unlimited electrical energy from the sun,” no. 2780, pp. 1990–1991, 1999.

[2] Bett et al., “Presented at the 24th European Photovoltaic Solar Energy Conference and Exhibition, 21-25 September 2009, Hamburg, Germany,” 2009, no. September, pp. 21–25.

[3] Harold J. Hovel, “Solar cells for terrestrial applications,” *Sci. direct*, vol. 19, no. 6, pp. 605–615, 1977.

[4] Kulkarni et al, “Rural Electrification through Renewable Energy Sources- An Overview of Challenges and Prospects,” vol. 5013, no. 3, pp. 384–389, 2014.

[5] Herzog et al, “Perspective and Overview of Life Support systems and Sustainable Development.”

[6] N. Lior, “Sustainable energy development: The present (2009) situation and possible paths to the future,” *Energy*, vol. 35, no. 10, pp. 3976–3994, Oct. 2010.

[7] Ye et al, “Design, Fabrication, and Modification of Cost-Effective Nanostructured TiO2 for Solar Energy Applications,” Springer London, London, 2014.

[8] S. J.L., “Photovoltaics: Unlimited electrical energy from the sun,” *Phys. Today*, p. 22, 1993.

[9] Backus, “Solar Cell,” *IEEE Press. York*, 1980.

[10] E.V. Appleton, “Appleton,” *Nat. 3966535*, 1945.

[11] M. Igbal, *An Introduction to Solar Radiation*. Academic Press, 1983, p. Chap.3.

[12] F. Jay (ed), “IEEE Standard Dictionary of Electrical and Electronics Terms.” The Institute of Electrical and Electronic Engineers, Inc. New York, 1977.

[13] A. Oliva-Chatelain et al., “An Introduction to Solar Cell Technology,” 2011. [Online]. Available: http://cnx.org/content/m41217/1.1/.

[14] V. Balema, “Alternative Energy Photovoltaics, Ionic Liquids, and MOFs,” *Mateial Matters*, vol. 4, no. 4, p. 1, 2009.

[15] D. M. Chaplin et al., “,” *J. Appl. Phys.*, vol. 25, p. 676, 1954.

[16] D. M. Chaplin et al., in *US patent number 2780*, 1957.

[17] M. A. Green et al., "Solar cell ef fi ciency tables (version 43)," pp. 1–9, 2014.

[18] R. G. Nrel, *AUGUST 2010 2009 Renewable Energy Data Book*, no. August 2010. 2010, pp. 1–132.

[19] Kojima et al., "Novel photoelectrochemical cell with mesoscopic electrodes sensitized by lead-halide compounds (2). in Proc. 210th ECS Meeting.," 2006.

[20] Kojima et al., "Organometal halide perovskites as visible-light sensitizers for photovoltaic cells.," *J. Am. Chem. Soc.*, vol. 131, pp. 6050–6051, 2009.

[21] Zhou et al., "Interface engineering of highly efficient provskite solar cells," *Science (80-.).*, vol. 345, p. 542, 2014.

[22] Snaith et al., "The emergence of perovskite solar cells," *Nat. Photonics*, vol. 8, no. 7, pp. 506–514, Jun. 2014.

[23] M. Liu et al, "Efficient planar heterojunction perovskite solar cells by vapour deposition.," *Nature*, vol. 501, no. 7467, pp. 395–8, Sep. 2013.

[24] J. Burschka et al., "Sequential deposition as a route to high-performance perovskite-sensitized solar cells.," *Nature*, vol. 499, no. 7458, pp. 316–9, Jul. 2013.

[25] Noel et al., "Lead-Free Organic-Inorganic Tin Halide Perovskites for Photovoltaic Applications," *Energy Environ. Sci.*, vol. 7, pp. 3061–3068, 2014.

[26] Burgelman et al, *SCAPS manual*, no. May. 2014.

[27] M. Zeman, *Introduction to photovoltaic solar energy*. pp. 1–139.

[28] Feng et al, "Lead-free solid-state organic–inorganic halide perovskite solar cells," *Nat. Photonics*, vol. 8, no. 6, pp. 489–494, May 2014.

[29] J. Nelson, *The Physics of Solar Cells*. Imperial College Press: London, 2003, pp. 1–325.

[30] Yella et al,*Science*, vol. 334, pp. 629–634, 2011.

[31] M. A. Green et al.,*Prog. Photovoltaics*, vol. 22, pp. 1–9, 2014.

[32] Borriello et al, "Ab initio investigation of hybrid organic-inorganic perovskites based on tin halides," *Phys. Rev. B*, vol. 77, no. 23, p. 235214, 2008.

[33] Kagan et al, "Organic-inorganic hybrid materials as semiconducting channels in thin-film field-effect transistors," *Science*, vol. 286, no. 5441, pp. 945–947, 1999.

[34] A. M. Glazer, “The classification of tilted octahedra in perovskites,” *Acta Crystallogr. Sect. B Struct. Crystallogr. Cryst. Chem.*, vol. 28, no. 11, pp. 3384–3392, 1972.

[35] Mitzi et al, “Transport, Optical and Magnetic Properties of the conducting Halide Perovskite CH3NH3SnI3,” *J. Solid State Chem.*, vol. 114, pp. 159–163, 1995.

[36] Stoumpos et al, “Semiconducting tin and lead iodide perovskites with organic cations: phase transitions, high mobilities, and near-infrared photoluminescent properties.,” *Inorg. Chem.*, vol. 52, no. 15, pp. 9019–38, Aug. 2013.

[37] P. Umari et al, “Relativistic GW calculations on CH3NH3PbI3 and CH3NH3SnI3 perovskites for solar cell applications.,” *Sci. Rep.*, vol. 4, p. 4467, Jan. 2014.

[38] Fan et al, “Perovskite-based low-cost and high-efficiency hybrid halide solar cells,” *Photonics Res.*, vol. 2, no. 5, 2014.

[39] E. P. Giannelis, “Polymer layered silicate nanocomposites,” *Adv. Mater.*, vol. 8, no. 1, pp. 29–35, 1996.

[40] Okamoto et al, “Polymer/layered silicate nanocomposites: a review from preparation to processing,” *Prog. Polym. Sci.*, vol. 28, pp. 1539–1641, 2003.

[41] Etgar et al, “Mesoscopic CH3NH3PbI3/TiO2 heterojunction solar cells,” *J.Am. Chem. Soc.*, vol. 134, pp. 17396–17399, 2012.

[42] Chiarella et al, “Growth and characterization of hybrid (CnH2n+ 1NH3) 2CuCl4 self-assembled films,” *Cryst. Res. Technol.*, vol. 40, no. 10-11, pp. 1028–1032, 2005.

[43] Stranks et al, “Electron-hole diffusion lengths exceeding 1 micrometer in an organometal trihalide perovskite absorber,” *Science*, vol. 342, no. 6156, pp. 341–344, 2013.

[44] Wehrenfennig et al, “High charge carrier mobilities and lifetimes in organolead trihalide perovskites,” *Adv. Mater.*, vol. 26, no. 10, pp. 1584–1589, 2014.

[45] Liu et al, “Perovskite solar cells with a planar heterojunction structure prepared using room-temperature solution processing techniques,” *Nat. Photonics*, vol. 8, no. 2, pp. 133–138, Dec. 2013.

[46] Heo et al, “Solar cells containing perovskite compound and polymeric hole conductors,” *Nat. Photonics*, vol. 7, no. June, 2013.

[47] McGehee et al, “Novel inorganic-organic perovskites for solution processable photovoltaics.”

[48] Burgelman et. al., “Modelling polycrystalline semiconductor solar cells,” *Thin Solid Films*, vol. 361–362, pp. 527–532, Feb. 2000.

[49] Minemoto et al, “Device modeling of perovskite solar cells based on structural similarity with thin film inorganic semiconductor solar cells,” *J. Appl. Phys.*, vol. 116, no. 5, p. 054505, Aug. 2014.

[50] Edri et al, “Elucidating the charge carrier separation and working mechanism of CH3NH3PbI(3-x)Cl(x) perovskite solar cells.,” *Nat. Commun.*, vol. 5, p. 3461, Jan. 2014.

[51] Tanaka et al, “Comparative study on the excitons in lead-halide-based perovskite-type crystals CH3NH3PbBr3 CH3NH3PbI3,” *Sci. direct*, vol. 127, pp. 619–623, 2003.

[52] McGraw-Hill Concise, *Encyclopedia of Physics*. The McGraw-Hill Companies, Inc, 2002.

[53] Marc Burgelman et al., “Modeling Thin-film PV Devices,” *Prog. Photovoltaics*, vol. 12, pp. 143–153, 2004.

[54] R. F. Pierret, *Semiconductor Device Fundamentals*. 1996.

[55] D. Neamen, *Semiconducttor Physics and Devices*, 3rd ed. 2003.

[56] S.M. Sze, *Physics of Semiconductor Devices*. 2007.

[57] Liu et al, “Numerical simulation: Toward the design of high-efficiency planar perovskite solar cells,” *Appl. Phys. Lett.*, vol. 253508, no. 104, 2014.

[58] Movla et al., “Optik Optimization of the CIGS based thin film solar cells : Numerical simulation and analysis,” *Opt. - Int. J. Light Electron Opt.*, vol. 125, no. 1, pp. 67–70, 2014.

[59] M. Pope and C.E. Swenberg, *Electronic processes in organic crystals and polymers*, 2nd ed. Oxford, Univ. Press, 1999.